INVESTIGATION OF BIOCHEMICAL PROCESSES IN SINGLE CELL USING SURFACE-ENHANCED RAMAN SCATTERING
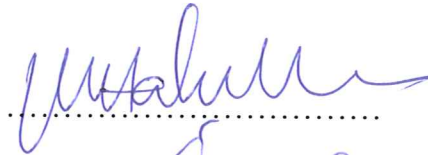
by

Deniz Yaşar Öztaş

Submitted to Graduate School of Natural and Applied Sciences

in Partial Fulfillment of the Requirements

for the Degree of Master of Science in

Biotechnology

Yeditepe University

2017

INVESTIGATION OF BIOCHEMICAL PROCESSES IN SINGLE CELL USING SURFACE-ENHANCED RAMAN SCATTERING
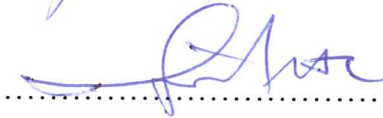
APPROVED BY:

Prof. Dr. Mustafa Çulha
(Thesis Supervisor)

Prof. Dr. Bahattin Yalçın

Assist. Prof. Dr. Hüseyin Çimen

DATE OF APPROVAL: ..../..../2017

ACKNOWLEDGEMENTS

ABSTRACT

INVESTIGATION OF BIOCHEMICAL PROCESSES IN SINGLE CELL USING SURFACE-ENHANCED RAMAN SCATTERING

Single cell analysis is rapidly emerging approach to gain molecular information at the individual cell level. Investigation of specific molecular mechanisms and pathways providing in single cell level is crucial. In this study, we investigated Surface-enhanced Raman scattering (SERS) to study single-cells. Gold nanoparticles (AuNPs) were used as routinely employed SERS substrate. SERS activity of AuNPs depends on size, shape and aggregation status in living cell depending on their uptake profile. We are interested in understanding the biochemical changes on AuNPs or in their aggregates to understand the possibility of monitoring cellular biochemical process in a living cell. Thus, two different sizes of AuNPs with two different surface chemistry were used in the study. The order and combination of AuNPs with different sizes and surface chemistry helped to understand the spectra obtained from a single cell and thus the nature of the biochemical processes taking place on the AuNPs surfaces. This study showed that SERS can be used for single cell analysis and its possible use in molecular biology. In this study, the spectral changes espicially correspond to protein and lipids were observed depending on size, surface chemistry, and aggregation status in time dependent manner.

ÖZET

TEK HÜCREDE GERÇEKLEŞEN BİYOKİMYASAL SÜRECİN YÜZEYCE ZENGİNLEŞTİRİLMİŞ RAMAN SAÇILMASI İLE İNCELENMESİ

Tek hücre analizi; tek hücre seviyesinde moleküler bilgi edinmek için gelişmekte olan bir yaklaşımdır. Özel moleküler mekanizmaları ve yollarını tek hücre seviyesinde incelemek oldukça önemlidir. Bu çalışmada tek hücre analizi için Yüzeyce zenginleştirilmiş Raman saçılması (YZRS) kullanılmıştır. YZRS alt maddesi olarak ise genel olarak kullanılmakta olan altın nanoparçacıkları kullanılmıştır. YZRS aktivitesi altın nanoparçacıkların boyutuna, şekline, ve hücre içi alımına göre birikimine bağlıdır. Biz bu çalışmada, canlı hücre içerisinde gerçekleşen biyokimyasal değişmeleri izlemek için altın nanoparçacıkların ya da kümeleleşmelerinin üzerindeki biyokimyasal değişmeleri YZRS ile anlamaya çalıştık. Bunun için, iki farklı boya ve yüzeye sahip altın nanoparçacıklar kullandık. Altın nanoparçacıkların farklı boy ve yüzey kimyası kombinasyonu; tek hücreden gelen Raman saçılımı ve böylelikle yüzeyde oluşan biyokimyasal değişiklikleri hakkında bilgi vermiştir. Bu çalışma tek hücreden gelen spectrayı anlamlandırmakta ve moleküler biyolojide ve tıpta kullanım olasılığını ortaya çıkarmakta yardımcı olmuştur. Çalışmamızda, özellikle protein ve yağları belirten; boyuta, yüzey kimyasına ve kümeleşme durumuna göre zamana bağlı saçılım değişimleri gözlemlenmiştir.

TABLE OF CONTENTS

LIST OF FIGURES

LIST OF TABLES

LIST OF SYMBOLS/ABBREVIATIONS

AFM	Atomic Force Microscopy
AgNPs	Silver Nanoparticles
AuNPs	Gold Nanoparticles
CCVs	Clathrin-coated vesicles
CdTe	Cadmium telluride
CTAB	Cetyl trimethylammonium bromide
CuO	Copper(II) oxide
CV	Coefficient of variation
CyTOF	Mass Cytometry
EGFR	Epidermal growth factor receptor
ESI	Electrospray ionization
FACS	Fluorescence activated cell sorting
Fe_3O_4	Iron(II,III) oxide
HCPT	Hydroxy camptothecin
HER2	Human Epidermal Growth Factor Receptor 2
HIV	Human immunodeficiency virus
MALBAC	Multiple annealing and looping-based amplification cycles
MALDI	Matrix-assisted laser desorption/ionization
MS	Mass spectrometry
nm	Nanometer
nM	Nanomolar
NPs	Nanoparticles
NMR	Nuclear magnetic resonance
NiO	Nickel(II) oxide
PALM	Photo-activated localization microscopy
PAH	Polycyclic aromatic hydrocarbon
PEG	Polyethylene glycol
PbS	Lead(II) sulfide
PDADMAC	Polydiallyldimethylammonium chloride
PVA	Polyvinyl alcohol

PSS	Poly(styrenesulfonate)
SCBCs	Single-cell barcode chips
SCGE	Single cell gel electrophoresis
scWestern	Single-cell western blotting
SERS	Surface enhanced-Raman Scattering
SiO_2	Silicon dioxide
STORM	Stochastic optical reconstruction microscopy
TEM	Transmission Electron Microscopy
TiO_2	Titanium dioxide
ZnO	Zinc oxide

1. INTRODUCTION

A cell is the basic unit of a living organism. Many abnormalities and diseases, especially cancer, arise due to intracellular biochemical changes [1]. However, cell populations are heterogeneous. Each cell type has a unique function and exhibits significant variations in proteins, transcripts, metabolites and other analytes. To obtain an accurate result from the analysis, all cells should be investigated individually [2]. Therefore, single cell analysis has emerged in order to obtain the molecular information at the single-cell level. When molecular signatures at the single-cell level can be measured, understanding the cellular specificity and complexity of a single cell becomes possible.

Single-cell analysis is used to investigate many topics, such as cancer, stem cells, immunology, and drug research and development. In cancer studies, molecular profiling of the subpopulations plays an important role in diagnosis and treatment of cancer. Full characterization of the cell populations can be achieved and also the stem cell differentiation mechanism can be identified using single-cell sequencing [3, 4]. In immunology studies, single-cell analysis overcomes the specific molecular marker limitation and makes the identification of unique gene expression patterns in T and B cells possible [5]. Also, single-cell analysis is used to measure the drug responses, which vary due to the heterogeneity [6].

There are many techniques that are used at the single-cell level and these techniques are constantly being improved. DNA sequencing, RNA sequencing, exome sequencing, and microarrays are some of the single-cell analysis techniques that are used for gene and transcript studies [7]. However, the main challenge, for these techniques is contamination.

Mass spectrometry (MS), mass cytometry (CyTOF), Nuclear magnetic resonance (NMR), flow cytometry and protein arrays are used for the protein and metabolic studies at the single-cell level [8, 9]. However, antibodies are required for these techniques, except MS, which has limitations including manual single-cell isolation and high amount of sample requirement.

Complete analysis of cellular function at the single-cell level requires analysis of nucleic acids, proteins, lipids, and functional analytes including kinases, apoptotic markers and metabolites. Analysis of every molecule requires a different technique. To overcome this

limitation, new techniques were developed, such as Raman spectroscopy. Chemical structure of a cell including nucleic acids, proteins, lipids can be determined using Raman spectroscopy without any labelling or staining procedure [10]. Therefore Raman spectroscopy is a suitable technique for live cell studies. since 1990 many cell studies were carried out using Raman spectroscopy [11]. However, the main disadvantage of Raman spectroscopy is the weak signals. To overcome this problem, surface enhanced-Raman scattering was developed, which uses Raman-active noble metal nanostructured surfaces or nanoparticles, more specifically gold or silver to enhance the Raman scattering [12].

SERS has been used in many fields including biomedical imaging, molecular sensing, and detection since its discovery. The first single-cell analysis using SERS was reported in 1991 by Nabiev et al. [13]. In the recent years, the use of SERS in single-cell analysis has regained attention.

For single-cell analysis, cells are incubated with nanoparticles to obtain the spectra. Therefore, cellular uptake of nanomaterials plays a very important role in SERS measurements. Uptake of nanoparticles which are smaller than ~200 nm is facilitated by clathrin-mediated endocytosis [14]. Endocytic vesicles known as clathrin-coated vesicles (CCVs) are formed by coated pits and clathrin. CCVs transport and recycle the molecules in the cells [15].

Since the cellular uptake depends on size, shape and surface chemistry of nanomaterials, SERS activity is also affected by these properties of the SERS substrates. For example, different sizes of AuNPs exhibit differences in the cellular uptake [14]. 50 nm nanoparticle is reported as the optimal size for the cellular uptake [16]. On the other hand, shape of the nanoparticle was also demonstrated to have an effect on the cellular uptake in many studies [17, 18]. For example, uptake of spherical nanoparticles is better than the uptake of rod-like nanoparticles [19]. The surface properties including charge and targeting receptor play important role in the endocytosis pathway of the nanoparticles. For example, positively charged nanoparticles are endocytosized more efficiently than the negatively charged nanoparticles [20].

In this study, we have utilized SERS to monitor the biochemical changes on AuNPs and AuNP clusters up-taken by cells. Our goal was to investigate the possibility of monitoring biochemical process in a living cell using the technique. First, 13 nm AuNPs (AuNPs13) and

50 nm AuNPs (AuNP50) were synthesized using Turkevich method [21] and the nanoparticles were characterized by UV/vis spectroscopy and dynamic light scattering (DLS). Then, both AuNPs13 and AuNP50 were modified with thiol modified poly-Adenine oligonucleotides. MDA-MB-231 cells were later exposed to a mixture of AuNPs13, AuNPs50, or oligonucleotide modified AuNPs (AuNPs13-Oligo or AuNPs50-Oligo). Then the SERS spectra of the NP exposed cells were collected after 4h, 8h, 12h, and 24h. At each time stamp, raster scans were performed on 20 cells to analyze the SERS spectra reproducibility. Using the changes in the spectra, the effects of NP size, surface chemistry and incubation time were analyzed to determine the most effective conditions for consistent single cell spectra measurements.

The results indicate that oligonucleotide modified AuNPs were up-taken by the cells more efficiently. The major changes in the SERS spectra were observed for the protein and lipid regions during the endocytosis. Different spectral changes were observed for each AuNPs treatment in the same incubation time. Therefore, it could be said that AuNPs13, AuNPs50, and oligonucleotide modified AuNPs could be used to investigate the different stages of endocytosis in a single-cell using SERS.

2. THEORETICAL BACKGROUND

2.1. MOLECULAR TECHNIQUES IN SINGLE CELL ANALYSIS

Individual cells may differ from each other even in the same population. During the cellular heterogeneity, tools and assays that are used for cell analysis do not give accurate results. Minor characteristics of the cells may be masked by the major characteristics [22]. Therefore, single cell analysis is crucial to illuminate the cellular diversity and heterogeneity. It makes collecting molecular information, molecular mechanisms and pathways at the individual cell level possible. These advantages have led to new approaches in many fields such as tissue engineering, biomedical research, and cancer biology. In addition to these, single cell analysis is promising for diagnostics and therapeutic applications. Some of the major techniques used for these applications are DNA sequencing, fiber-optic arrays, comet assay, mass spectrometry, and flow cytometry.

DNA sequencing has been developed in the recent years. The genome must be amplified by performing PCR-based whole-genome amplification methods before sequencing [23]. However, random genes may cause under-amplification problems during nonlinear PCR process [24]. To avoid these problems multiple displacement amplification method may be used alternatively. This method requires φ29 DNA polymerase. However, since φ29 DNA polymerase enzyme is nonlinear amplifier, it may cause bias. Another technique used for whole-genome amplification is multiple annealing and looping-based amplification cycles (MALBAC) [25]. Since initial genome amplification process is linear in MALBAC, amplification bias is reduced.

DNA sequencing has several challenges though. Firstly, isolation of individual cells should be precise. Secondly, amplification of the genome of a single cell should be enough for further studies. Thirdly, the process both should be cost effective, and it should also fulfill the requirements of the study. In addition to these, DNA sequencing methods could be deviated from the ideal uniform which creates the bias. The bias is the biggest challenge for this technique [26]. To avoid bias, experiment setups of DNA sequencing should be arranged and carried out carefully.

Another single cell analysis technique is called as RNA sequencing, which is also known as whole transcriptome shotgun sequencing. This next-generation sequencing tools technique is used to analyze the transcriptome at single-cell level [27]. Using RNA sequencing immune cells have been studied and transcriptional heterogeneity of healthy and diseased tissues have been identified [28-30]. However, contamination is a major challenge for this technique [31].
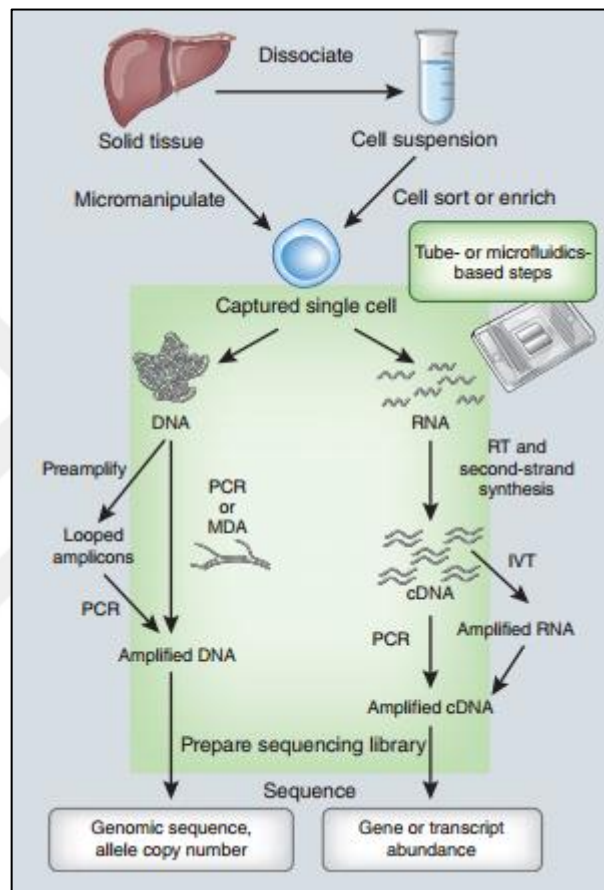
Figure 2.1. Workflows of RNA and DNA sequencing of a single cell [32].

Comet assay, also known as the single cell gel electrophoresis (SCGE), is a visual and sensitive technique that is used to measure the DNA breakage in mammalian cells at the single-cell level [33, 34]. However, using this technique only limited information can be gathered from measuring DNA breakage.

Mass spectrometry is another technique that is used to analyze the protein and metabolite at the single-cell level. Characterization of peptides has been achieved using MALDI MS and characterization of small molecules has been performed using electrospray ionization (ESI) MS [35, 36]. However, offline manual isolation is required; and lysis of a single cell is an another challenge for this technique.

Other than MS, Mass cytometry (CyTOF), Single-cell barcode chips (SCBCs), Microengraving, fluorescence activated cell sorting (FACS), Single-cell western blotting (scWestern) methods can be used for single-cell proteomic analysis [37-40]. Each of these techniques is used for a different purpose. FACs is used to analyze and sort the cells based on cell surface markers. CyTOF and SCBCs are used to analyze the functional cytoplasmic proteins. And ScWestern is a western blotting assay which has originated from comet assays. Although these techniques have certain advantages, they also have some disadvantages such as further analysis, use of antibodies, and an experienced operator requirements.

Beyond the molecular techniques, new approaches have emerged such as atomic force microscopy (AFM), fluorescence microscopy, and Raman spectroscopy. For example, the effect of paclitaxel on the Ishikawa and HeLa cells and the relationship between the morphology and biophysical properties have been observed using AFM [41]. Cells were stained with fluorescent molecules, so that they can be visualized by Fluorescence microscopy. With more developed techniques such as STORM (stochastic optical reconstruction microscopy) or PALM (photo-activated localization microscopy), higher resolutions can be achieved[42].

Despite their advantages, all the techniques that we have discussed so far, have certain problems and limitations. To overcome these limitations Raman spectroscopy is a good alternative for live cell imaging. The basics of the technique and its use in single-cell analysis will be summarized below.

2.2. RAMAN SPECTROSCOPY

Spectroscopy is the study of interaction of light with matter. Absorption, transmission and scattering occur when light interacts with matter. One of the scattering phenomenon is Raman, which was discovered by C.V. Raman in 1928 [43]. Working principle of Raman spectroscopy based on inelastic scattering of monochromatic light and vibrational (phonon) states of molecules which interact each other and illuminate the sample [44].

Scattering occurs in all directions when monochromatic light strikes and interacts with molecules. Most of the scattered light have frequency that equals to frequency of incident radiation which creates the Rayleigh scattering, the less amount of scattered light has frequency that differs from frequency of incident radiation which creates the Raman scattering [45]. When photons interact with sample energy can be lost which creates stokes scattering or energy can be gained which creates anti-stokes scattering [46]. The energy diagram of Raman scattering is shown in Figure 1.
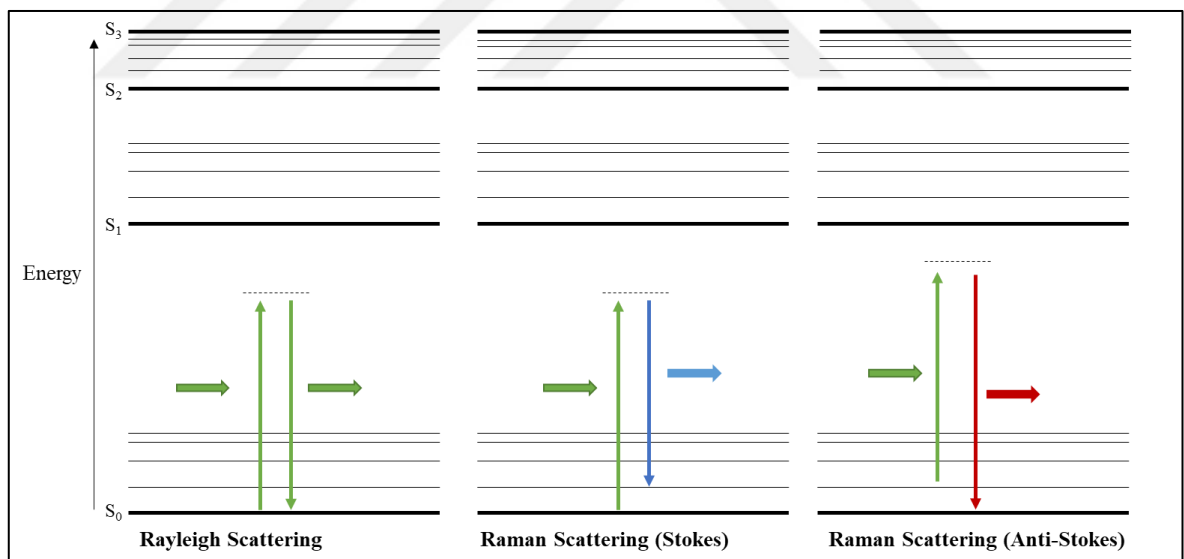
Figure 2.2. Energy diagram of Rayleigh and Raman scattering with different energy levels (S_0, S_1, S_2, S_3).

Raman spectroscopy is a technique that provides information about biological and non-biological molecules and their structures. The main advantages of Raman spectroscopy are being non-destructive and label-free technique.

2.2.1. Raman Spectroscopy In Single Cell Analysis

Chemical structure of a cell including nucleic acids, lipid, and proteins can be observed without any labelling or staining using Raman spectroscopy [10]. In first reports of Raman spectroscopy used for single-cell analysis, cells were fixed with alcohols and aldehydes to prevent the degradation. Alcohols were used to disrupt the hydrophobic bonds and denature the proteins; aldehydes were used to induce the covalent bonds between proteins [47]. Compartments of the cells including nucleic acids [48], proteins [49], lipids [50], and mitochondria [51] were monitored by using Raman spectroscopy with cell fixation procedures. Also, cell cycle was observed at different phases [52] and identification of differences between the benign and malignant breast tissues were achieved using fixed cells. [53] However, researchers demonstrated that fixing procedures could affect the Raman spectra of the cells. The Raman spectra differences of nucleic acids, lipids and proteins between fixed and unfixed cell were investigated [54]. Also, in other studies, changes in Raman spectra of proteins and nucleic acids depending on fixation procedures were demonstrated [55, 56].

Since discovery of cell fixation effects, cells have been investigated without cell-fixation procedures. For example, effects of doxorubicin with different exposure times to single lymphocytes were investigated using Raman spectroscopy without any fixation, staining or labeling [57]. Also, cell cycle phases of human embryonic stem cells were observed without any labelling and fixation [58].

Although Raman spectroscopy has many advantages, it is not widely used in clinical research because of its inherently weak signals [59]. To overcome this problem laser power and exposure time are increased to obtain strong signals from samples. However, samples were damaged because of increased laser power and exposure time [60]. Therefore, new techniques such as combination with standard confocal microscope and surface-enhanced Raman spectroscopy have been developed to enhance the weak signals without any damage [11, 61].

2.3. SURFACE ENHANCED RAMAN SCATTERING

Surface-enhanced Raman scattering (SERS) is emerged to enhance the intensity of Raman scattering by using Raman-active molecules or nanoscale roughened metal surfaces such as gold (Au) and silver (Ag). Their laser excitation drives the surface charges resonantly and plasmonic light field is created [62]. Absorption of a molecule close to the enhanced field is enough to observe the enhancement in Raman intensity. Enhancement factors can be remained higher depending on molecules [22]. Therefore, very small concentration of substances can be detected and identified due to improved limit of detection; even single molecule can be detected under favor of high Enhancement factors.

The first enhanced Raman signal of pyridine was observed in 1974 using rough silver film [63]. However, many of enhanced Raman signals were observed from corrugated surface of the electrode. Since the discovery of SERS by Van Duyne in 1977, research interest of SERS substrates have been remained for 40 years [64].

The enhancement factors of SERS depend on the substrates [12]. The mechanisms of enhancement factors are divided into the two which are electromagnetic field enhancement and chemical enhancement mechanism [65]. In chemical enhancement mechanism, there is charge transferring between the adsorbed molecule and metal to enhance the molecular vibration. Theoretically, chemical enhancement factors are calculated up to 10^3 [66] while the electromagnetic enhancement factors can be reached to 10^{10}-10^{11} under favor of localized surface plasmons (LSPs) of metallic nanostructure [67].

2.3.1. SERS Substrates

Semiconductor substrates, and noble metals are used as SERS-active substrates. Semiconductor substrates were firstly used in 1983; enhancement of the pyridine spectrum was observed the using NiO [68]. Later, similar enhancement effects using TiO_2 [69] were observed and later ZnO, CuO, Fe_3O_4, PbS, and CdTe were used as SERS-active substrates [70-74]. Also, graphene-based SERS substrates are emerged in recent years [75].

Au and Ag nanoparticles are widely used as SERS-active substrates because of their high Surface Plasmon Resonance (SPR) which occur when oscillation of free surface electrons induced by light [76].
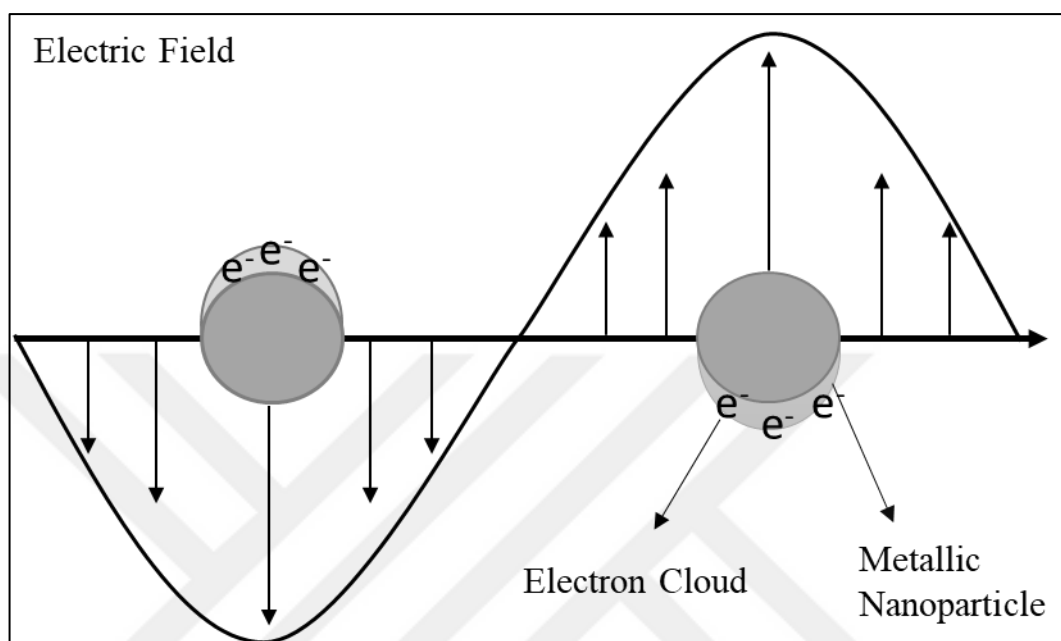
Figure 2.3. **S**urface plasmon resonance (SPR) for a metallic nanoparticle.

Preparation of gold and silver nanoparticles was achieved by reducing reactions [61]. The main disadvantage of bare AuNPs and AgNPs is oxidation. To overcome the problems such as instability, oxidation and aggregation of nanoparticles for SERS measurements, Au and Ag nanoparticles are coated with shells. Silica coating is a method to improve core/shell nanostructures [77]. Silica-coated plasmonic cores were fabricated and embedded with Raman probes to be used as SERS-active substrates [78]. Also, silica-encapsulated Ag (Ag@SiO2) was developed using environmental friendly solvents. To detect the biomolecules, SERS-active substrates with core-shell structure have been used and they have exhibited stability [79].

It is well known that AgNPs have higher enhancement factors than AuNPs [80]. However, AgNPs should not be used in bioanalysis because of is toxicity. Therefore, AuNPs are widely used in bioanalysis as SERS-active substrates due to the its bio-compatibility and non-toxicity [81]. AuNPs have unique optical properties and chemical stability, therefore AuNPs are widely used in scientific and technological fields such as chemical and biosensing, biomedical imaging, and drug delivery. Different shapes of AuNPs such as spheres, rods, wires, cubes, stars and triangles have been used for specific biomedical applications [82].

However, before the use of gold nanoparticles in biomedical and medicine applications, its potential toxicity should be investigated. For this reason, toxicity of AuNPs *in vivo* and *in vitro* has been investigated in many research and toxicity of AuNPs will be summarized below [83].

2.3.1.1 Toxicity of Gold Nanoparticles

Bulk gold is known as chemically inert and safe [84]. Therefore, gold nanoparticles and gold based molecules are used in bioimaging and therapeutic applications. However, nanoparticles can cause the DNA damage, apoptosis, oxidative stress and organelle damage at the cellular level but gold nanoparticles have been reported as non-toxic in many studies [85]. Goodman et al. reported that gold nanoparticles are toxic. However, in the same study, anionic AuNPs were found as non-toxic. While 2 nm of cationic gold nanospheres have been found as toxic, the same nanoparticles which have negative surface charge were found non-toxic by using same concentration [86]. In another study, necrosis was triggered by 1.4 nm gold nanospheres while there was no any cellular damage for 15 nm AuNPs [87]. Because of different size, shape, and surface chemistry of gold nanoparticles, toxicity of AuNPs may vary.

AuNPs in the range of 4 nm to 100 nm are widely used in cell studies. Since different reducing agents are used to synthesise different size of AuNPs, toxicity of reducing agents are important to understand the toxicity of AuNPs. For example, rod shaped AuNPs which synthesised using Cetyltrimethylammonium bromide is toxic. However, use of Au nanorods as SERS-active substrate in biological applications was reported [88].

To overcome the toxicity, AuNPs have been modified. Modification of AuNPs also enables the targeting or delivering. However, when size, shape and surface chemistry of AuNPs change, its cellular uptake, toxicity and also SERS activity changed [89].

2.3.1.2 Size-dependent endocytosis of Gold Nanoparticles

The endocytosis process of AuNPs is important to understand for drug delivery, toxicity, clinical diagnostics and therapeutics and many other biomedical applications. Endocytosis of AuNPs was found to be size-dependent in many research [90].

Small molecules such as ions, amino acids, and sugars can traverse the plasma membrane using integral membrane protein pumps or channels. On the other hand, the macromolecules can be carried into the cell using vesicles which are derived from membrane by invagination and pinching-off. This process is called as endocytosis [15]. Different endocytic pathways take role in regard to the size of the endocytic vesicles.

Endocytosis can be divided into two categories; 'phagocytosis' and 'pinocytosis'. Pinocytosis has four basic mechanisms; clathrin-mediated endocytosis (CME), caveolae-mediated endocytosis, clathrin- and caveolae- independent, and micropinocytosis that are shown in Figure 2.4.
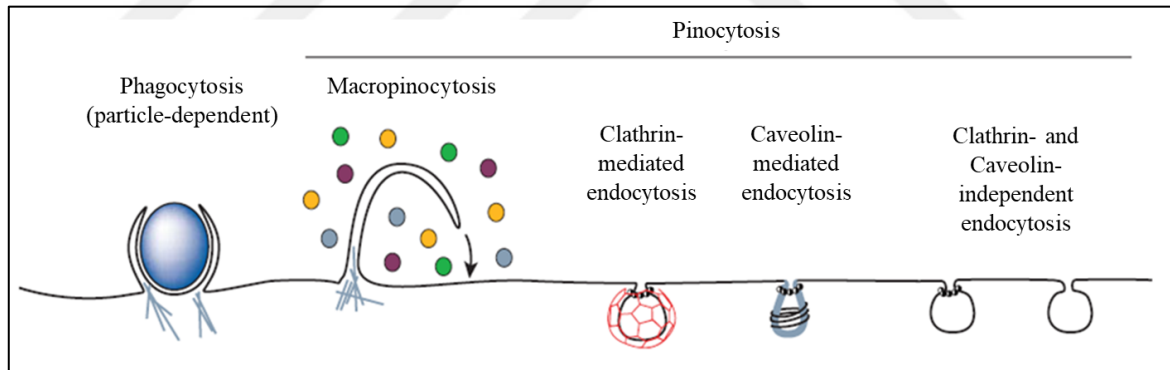
Figure 2.4. Different endocytosic pathways of NPs cellular uptake [15].

Phagocytosis is an active and highly regulated process to clear the pathogens or large molecules. Specific cell-surface receptors and signalling cascades are mediated by Rho-family GTPases [91]. Membrane ruffling is induced by growth factors or other signals for macropinocytosis process which is also mediated by Rho-family GTPases.

Caveolae which mediate the cellular transport of proteins are flask-shaped invaginations of the plasma membrane. Their shapes and structures are mediated by caveolin which is a integral membrane protein [92]. Caveolin form a caveolin coat on the surface of the

membrane invaginations, internalized and vesicles carry the particles. Entry of nanoparticles with approximately 500 nm size is utilized by caveolae-mediated endocytosis [14].

Clathrin-mediated endocytosis is an another vesicular cellular transport. Signal transduction and nutrient import are induced by internalization and recycling of receptors thus synaptic vesicles are reformed [93]. Entry of nanoparticles which are under 200 nm is utilized by clathrin-mediated endocytosis [14].

On the other hand, small structures which have approximately 40-50 nm size, diffuse freely on the cell surface. This type of endocytosis is called as Clathrin- and caveolin-independent endocytosis [94].

Table 2.1. summarizes the cellular uptake and toxicity of AuNPs depending on size, shape and modification.

Table 2.1. Summary of influence of AuNP size, shape, and surface chemistry on toxicity and cellular uptake.

AuNPs Size/Shape	Surface Chemistry	Cell Line	Toxicity	Uptake Efficiency
2, 4, and 6 nm / Spherical	Cationic, neutral and anionic	Human cervical cells (HeLa)	90 per cent cell viability after 24 h	More uptake efficiency for cationic nanoparticles, less for neutral and anionic particles [95].
17.7 nm / Spherical	Citrate, PAH, PVA	Breast cancer cells (SK-BR-3)	90 per cent cell viability after 24 h	AuNPs/cell; 900 for PVA,1.800 for citrate, 5.200 for PAH [96].
10, 25, and 50 nm / Spherical	HCPT	Human breast cancer cells (MDA-MB-23)	73.4±4.5 per cent cell viability after 24 h	Higher uptake efficiency for 50 nm [97].

50 x 20 / Rods	CTAB, PEG, anti-HER2	SK-BR-3	90 per cent cell viability after 24 h	AuNPs/cell; 3,000 for PEG, 4,400 for anti-HER2, 8,000 for CTAB [98].
50x20 / Cage	Anti-EGFR, PEG	Human brain cells (U-87 MG)	Non-toxic	AuNPs/cell; 190 ± 31 for PEG and 826 ± 50 for anti-EGFR [99].
40x18 / Rods	CTAB, PAH, PSS, PDADMAC	HeLa	90 per cent cell viability after 24 h	AuNPs/cell; 1.000 for PSS 12.000 for PAH, 12.000 for CTAB, 150.000 for PDADMAC [100].

2.3.2. SERS in Molecular Sensing

SERS is a technique which can be used as a sensitive and label-free biosensor for detection and identification of small molecules including DNA, proteins, lipids. Also, SERS can be used for cellular sensing [101]. To detect and identify the desired molecule from the complex area, SERS molecular sensors have been emerged.

Biological molecules can be identified in the range of 400 cm^{-1} to 1400 cm^{-1} wavelength. For example, phosphate groups of DNA are detected at 980 cm^{-1}, 1080 cm^{-1} and 1240 cm^{-1} while the carbonhydrates are detected at 470 cm^{-1} and 1200 cm^{-1} [102, 103]. Knowledge of information of the molecules provides us to use the SERS for sensing, detection and identification.

For various applications, SERS can be used as a biosensor. For example, SERS was utilized for a pathogen detection using Ag nanorods in 2002. In this study, different SERS spectra were obtained from different viruses including adenovirus, rhinovirus and HIV according to the their compositions [104]. In another study, bacterial cells were detected using gold

nanoparticle covered SiO_2 substrates by Ziegler's group [105]. Also, ultrasensitive sensing of bacteria and HIV DNA without any labelling was reported using SERS[106]. These studies demonstrated that SERS can be used to detect the pathogens instead of long molecular techniques such as PCR. Differently from these, DNA hybridization was observed without labelling using SERS. To detect the target sequence, 2-aminopurine was substituted for adenine in the probe DNA sequence [107].

The cell surface was investigate in many research using SERS. For example, the binding potential of cell-surface receptors was investigated using SERS. For this study, Human glioma (U251) and epidermoid tumors (A431) were used and epidermal growth factor receptor (EGFR) was chosen for the sensing. EGFR-targeted and untargeted NPs were prepared as SERS substrate and the tissues were stained using prepared NPs. Therefore, they figured out that binding potential depends the NP concentration on cell-surface and the results were checked using flow cytometry [108]. MUC1 mucin and nucleolin were detected on the MCF-7 cell by Li et al. using DNA–gold nanoaggregates structure [109].

In another study, membrane proteins on cells were monitored using SERS [110]. Surface of HeLa cells were labelled with cyano probe functionalized silver nanoparticles (NPs) for this study. These studies demonstrated that SERS can be used to monitor the cell-surface receptors and proteins and used for detection of the changes on the cell-surface.

2.4. SERS IN SINGLE CELL ANALYSIS

The first single-cell analysis using SERS was reported in 1991. Interaction of doxorubicin with the cells was observed using AgNPs as SERS substrate [13]. Later, AuNPs were utilized as SERS-active substrate for the single-cell analysis in 2002 by Kneipp's group [111]. In the process of time, different size, shape and surface chemistry of AuNPs have been used as SERS-active substrate in single-cell analysis. For example, gold nanorods (AuNRs) were conjugated with anti-EGFR and used as cancer cell diagnostics tool in 2007 [112] while the bare AuNPs were used to investigate the cell response to different doses of nanomaterials at the single-cell level [113]. Small molecules such as glucose, NADPH/NADP$^+$, and polyamines were detected in HeLa cells using AuNP - AuNR nanostructures instead of immunoassay approaches [114].

Cellular processes such as metabolism, cell growth, and cell membrane polarity depending on pH were investigated using SERS [115]. Spherical AuNPs were modified with pH responsive 4-mercaptobenzoic acid (MBA). In this study, SERS signal at 1720 cm^{-1} that corresponds to symmetric stretching of the COO$^-$ group is increased responsing acidic pH. But in neutral and alkaline environments, SERS peak at 1400 cm^{-1} that corresponds to C=O bond is increased due to deprotonation of COO$^-$ group. Also, pH changes of live cells were successfully monitored using BSA coated [116].

In recent study, intracellular adhesion molecule-1 (ICAM-1) which released after the treatment of lipopolysaccharide (LPS) in murine macrophage cells (Raw264.7) were detected using SERS at the single-cell level. For this study, AuNRs containing 4-mercaptobenzoic acid were used [117]. The study indicates that SERS has high sensitivity and can be used to detect the biomarker molecules instead of ELISA techniques.

In another study, telomerase activity was detected and inhibition of telomerase activity by 3'-azido-3'-deoxythymidine was successfully measured at single-cell level using SERS [118].

Folate binding proteins in cancer HeLa and PC-3, and normal HaCaT cell lines were investigated using SERS at single-cell level [119]. To detect the expression, AuNPs were functionalized with folic acid and they bonded more on surface of cancer cell lines than the normal cell lines thus strong SERS signals were collected from cancer cells. Also, the Jurkat

cells and Raji cells were identified using AuNPs capped with 4-mercaptobenzoic acid (MBA) and antibody [120]. This study demonstrated that SERS can be useful technique to diagnose the leukemic lymphocytes at early stage.

MDA-MB-231 and MCF-7 breast cancer cell lines were characterized and distinguished using SERS by Hossains et al. [121]. Gold nanosphere deposited ITO was used as SERS substrates. They reported that molecular detection and distinguishing of the different cells can be achieved using SERS at single-cell level. Also, different types of breast cancer cells were distinguished using SERS at the single-cell level by Aberasturi et al. [122].

On the other hand, to monitor the cell differentiation and cell cycle phases, SERS technique was used in various studies. For example, differentiation of neural stem cells (NSCs) were observed. While the differentiated and undifferentiated NSCs were distinguished using graphene oxide (GO)-encapsulated gold nanoparticles by Kim et al. and differentiation of NSCs was monitored using gold nanostar arrays by El-Said et al. [123, 124].

To obtain the highest selectivity and sensitivity, SERS can be used at the single-cell level for the detection of targeted molecules. For example, mitochondria was targeted using AuNP-DNA core Au shell NPs. Cell death was induced by potassium cyanide (KCN) and they observed the spectral changes originating from mitochondria. It was demonstrated that SERS can be used to monitor the biochemical changes in mitochondria by targeting SERS substrates towards the compartments in a single-cell [125].

In another study, nucleus was targeted with different functionalized SERS substrates to investigate the biochemical changes using SERS. Gold nanorods were attached with a simian virus (SV40) nuclear localization signal (NLS) peptides through a thioalkyl-triazole linker by El-Sayed's group in 2007 [126]. They monitored the intracellular localization of modified gold nanorods using conventional microscope in the dark field. In addition to this, they investigate the biochemical environment of nanorods in nucleus using SERS and they figured out some spectral differences of normal and cancer cells. Also, 40 nm AuNPs attached with SV40 NLS were used to monitor the differentiation of neuroblastoma cells using SERS [127].

Different from those, to observe the efficiency of anti-cancer drugs, cisplatin and 5-fluorouracil, AuNPs were modified with NLS and Arginyl-glycyl-aspartic acid (RGD) peptides [128]. They reported that the Raman peaks at 1000 cm^{-1} and 1585 cm^{-1} which correspond the phenylalanine and DNA bases were increased during the cell death. Also, molecular changes in the nucleus were monitored using AuNPs modified NLS-peptide by El-Sayed's group [129]. Therefore, these studies demonstrate that SERS can be used to monitor the biochemical changes and intracellular molecular sensing at the targeted areas at single-cell level.

3. MATERIALS

3.1. CHEMICALS AND REAGENTS

3.1.1. AuNPs Preparation

Gold (III) chloride trihydrate (HAuCl$_4$·3H$_2$O, MW:393.83 g/mol) (Sigma-Aldrich #520918, USA), trisodium citrate dihydrate (C$_6$H$_5$Na$_3$O$_7$·2H$_2$O, MW:294.10 g/mol) (Merck #A829748, Germany).

3.1.2. Modification of AuNPs-Oligo

Potassium phosphate monobasic (KH$_2$PO$_4$, 85per cent, d:1.71 g/cm3, stock: 14.8 M; Merck #100573 Germany), potassium phosphate dibasic (K$_2$HPO$_4$, MW:174.18 g/mol) (Sigma-Aldrich P3786 USA), sodium chloride (NaCl, MW: 58.44 g/mol) (Sigma-Aldrich #31434, USA), sodium dodecyl sulphate (SDS) (C$_{12}$H$_{25}$O$_4$SNa, MW:288.38g/mol) (Bio Basic Inc. #151213 Canada), and oligonucleotides from Alpha DNA, Canada were used to modify the AuNPs with oligonucleotides.

3.1.3. Cell Culture

Dulbecco's Modified Eagle's Medium - High Glucose (Gibco #21063029, USA), fetal bovine serum (FBS) (Gibco #10270, UK), phosphate buffered saline (PBS) (HyClone™, USA) (Gibco #SH30256, USA), Penicillin Streptomycin (Gibco #15140122, USA), Trypsin-EDTA 0.25 per cent (Gibco #25200056, UK), Cell Proliferation Reagent WST-1 (Roche #05015944001, USA) were used for cell culture studies. Calcium fluoride (CaF$_2$) slides were used for the cell droplet.

3.2. INSTRUMENTS

Raman microscopy system (InVia Reflex, Renishaw, UK), UV/Vis spectrometer (PerkinElmer, USA), Zetasizer Nano-ZS (Malvern Insturements, UK). 2-5 centrifuge (Sigma, UK), ultrasonic bath (Bandelin Sonorex, Germany), mikro 22R centrifuge (Hettich, UK), Biohazard safety cabinet (Esco Class II type A2, USA), CO_2 incubator (37°C, CO_2 5per cent, Nuaire, USA), ELx800 Absorbance Reader (Biotek, USA) were used in this study.

3.3. CELL LINES

MDA-MB-231 breast cancer cell lines were purchased from American Type Culture Collection (Manassas, VA, USA).

4. METHODS

4.1. SYNTHESIS OF GOLD NANOPARTICLES

Two different sizes of AuNPs with an average size of 13 nm (AuNPs13) and 50 nm (AuNPs50) were synthesized using Turkevich method[21]. Before the synthesis all glasses were washed with aqua regia (HCl:HNO$_3$ of 3:1) to clean the surface of glass.

For the synthesis of AuNPs13, 40 mg of gold chloride (HAuCl$_4$.3H$_2$O) was dissolved in 100 ml ddH$_2$O. The solution was heated under stirring until boiling. Then, 10 mL of 38.8 mM sodium citrate (Na$_3$C$_6$H$_5$O$_7$) solution was added into the solution quickly. The soluiton was boiled for 15 minutes and waited at room temperature for cooling.

For the synthesis of AuNPs50, 10 mg of HAuCl$_4$.3H$_2$O was dissolved in 100 ml ddH$_2$O. The solution was heated under stirring until boiling. Then, one mL of one per cent Na$_3$C$_6$H$_5$O$_7$ solution was added into the solution quickly to the boiling solution. The soluiton was boiled for 15 minutes and waited at room temperature for cooling.

4.2. MODIFICATION OF GOLD NANOPARTICLES WITH OLIGONUCLEOTIDES

Both the AuNPs (AuNPs13 and AuNPs50) were modified with oligonucleotides using salt aging procedure[130]. Briefly, 100 µl of 0.1 M of phosphate buffer and 100 µl of 0.1 per cent SDS were added into one mL of each AuNPs13 and AuNPs50. A 20 µl of 100 µM 5'-thiol modified 20-mer polyadenine oligonucleotide (5'-SH-AAAAAAAAAAAAAAAAAAAA) was added into the AuNPs13 suspension while 30 µl of oligonucleotide was added to AuNPs50 suspension. Both the suspensions were mixed gently for 30 minutes at room temperature. After mixing, 100 µl of 2M NaCl solution was added into prepared suspensions at the three steps. After every addition step, the suspensions were sonicated for 20 seconds and mixed gently for 30 minutes. After the last addition of NaCl, the suspensions were incubated under gently mixing overnight. To remove excess

oligonucleotides, suspensions were centrifuged at 13.000 rpm for 20 minutes and the pellet was resuspended with ddH_2O. This step was repeated three times.

4.3. CHARACTARIZATION OF GOLD NANOPARTICLES AND GOLD NANOPARTICLES WITH OLIGONUCLEOTIDES

4.3.1. UV/Vis Spectroscopy

The absorbance of 13 nm AuNPs, 50 nm AuNPs, and AuNPs-Oligo were measured using UV/Vis spectrometer (PerkinElmer, USA).

4.3.2. Dynamic Light Scattering

Hydrodynamic size measurements of the 13 nm AuNPs, 50 nm AuNPs, and AuNPs-Oligo were measured using Zetasizer Nano-ZS (Malvern, UK) at the room temperature at 173° scattering angle with a 4 mW He–Ne laser. The prepared samples were placed into polystyrene cuvettes for the measurements. The refractive index and absorption of the AuNPs were assumed as 2.0 and 0.320, respectively. The measurements were repeated three times.

4.3.3. Transmission Electron Microscopy Analysis

Transmission Electron Microscopy (TEM) measurements of 13 nm AuNPs and 50 nm AuNPs were performed by using JEOL-2100 HRTEM LaB_6 (JEOL, USA) which is equipped with an Oxford Instruments 6498 EDS system operating at 200 kV. For the analysis, drop of samples were placed onto carbon support film coated copper TEM grids.

4.4. CELL CULTURE

MDA-MB-231 breast cancer cell line was cultured in high glucose DMEM containing 10 per cent FBS and 1 per cent PS at 37°C under 5 per cent CO_2 humidified atmosphere. In every 3-4 days cells were passaged and seeded again for reproducing.

4.5. TREATMENT OF CELLS WITH AUNPS

MDA-MB-231 cells were seeded at the density of 20.000 cells/well in 24-well plates. The cells were incubated for 24 h for attachment. After 24 h, the MDA-MB-231 cells were treated with AuNPs50, AuNPs50-Oligo at the concentration of 10 nM in cell culture medium. The treatment of cells by the mixtures of AuNPs was performed by addition of 25 nM of AuNPs50 and 10 nM of AuNPs13, and 25 nM of AuNPs50 and 10 nM of AuNPs13-Oligo into the cell culture medium.

4.6. WST-1 CELL VIABILITY ASSAY

Cytotoxicity of AuNPs13, AuNPs13-Oligo, AuNPs50, AuNPs50-Oligo, mixture of AuNPs50 and AuNPs13, and mixture of AuNPs50 and AuNPs13-Oligo were investigated by measuring the mitochondrial activiy using WST-1 assay. Briefly, MDA-MB-231 cells were seeded at the density of 5.000 cells/well in 96-well plates.After 24 h incubation, the MDA-MB-231 cells were treated with AuNPs13, AuNPs13-Oligo, AuNPs50, AuNPs50-Oligo, mixture of AuNPs50 and AuNPs13 and mixture of AuNPs50 and AuNPs13-Oligo at concentrations of 2.5, 5, 10, 15, 20, and 25 nM. After 24 h treatment, the cells were incubated with 5 per cent WST-1 dye containing fresh cell culture medium for 1.5 h. When the colour of medium returned to yellow from pink, cell viability was measured by using microplate reader at 450 nm.

4.7. SERS MEASUREMENTS

Cells were treated with the AuNPs for 4 h, 8 h, 12 h, and 24 h. After each incubation duration, the cells were detached from cell culture plate surface using trypsin and placed on CaF_2 within a volume of cell culture medium in order to prevent from drying. The cells were allowed to settle down on CaF_2 surface for a while in order to keep laser beam on the same sample without any flow. An area was selected for the SERS acqusition. Before the measurements, the system was calibrated using silicon as Raman shift standard at 520 cm^{-1}. A raster scan was performed with 2 μm steps using Raman Microscopy system with StreamLine™ under long distance 20X (N.A:0.4) objective at 830 nm excitation wavelength. The steps were determined according to the spot size of laser beam on sample surface, which was found as 2.5 μm from the formula 1.22 λ/NA. Approximately, 36-64 spectra were collected from a single cells. For all measurements, laser power of 150 mW and 2 s of exposure time were used as previously optimized by Kuku et al. in another study for single-cell analysis [113]. 20 cells were used for the evaluation and the spectra were processed using Wire software.
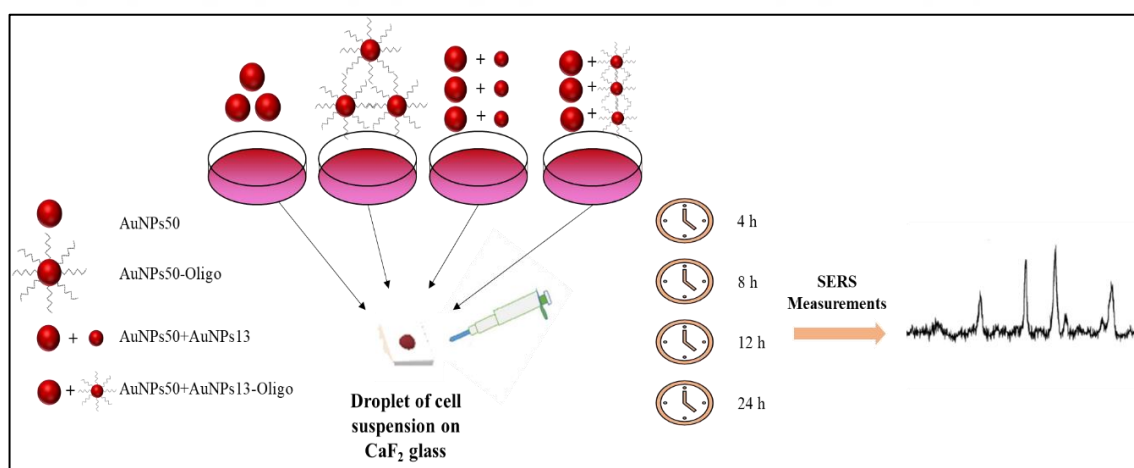
Figure 4.1 Experimental design of treatment and SERS measurements.

5. RESULTS AND DISCUSSION

5.1. CHARACTARIZATION OF GOLD NANOPARTICLES AND GOLD NANOPARTICLES WITH OLIGONUCLEOTIDES

Characterizations of AuNPs13, AuNPs50, AuNPs13-Oligo, and AuNPs50-Oligo were performed using UV/Vis spectroscopy and Dynamic Light Scattering (DLS).

5.1.1. UV/Vis Spectroscopy

The UV-Vis spectra of the AuNPs13 and AuNPs13-Oligo are shown in Figure 5.1. According to the literature, maximum wavelength for the AuNPs13 is at 520 nm[131]. When the AuNPs13 were modified with oligonucleotides, maximum wavelength shifted from 520 nm to 535 nm due to the modification and size increase.
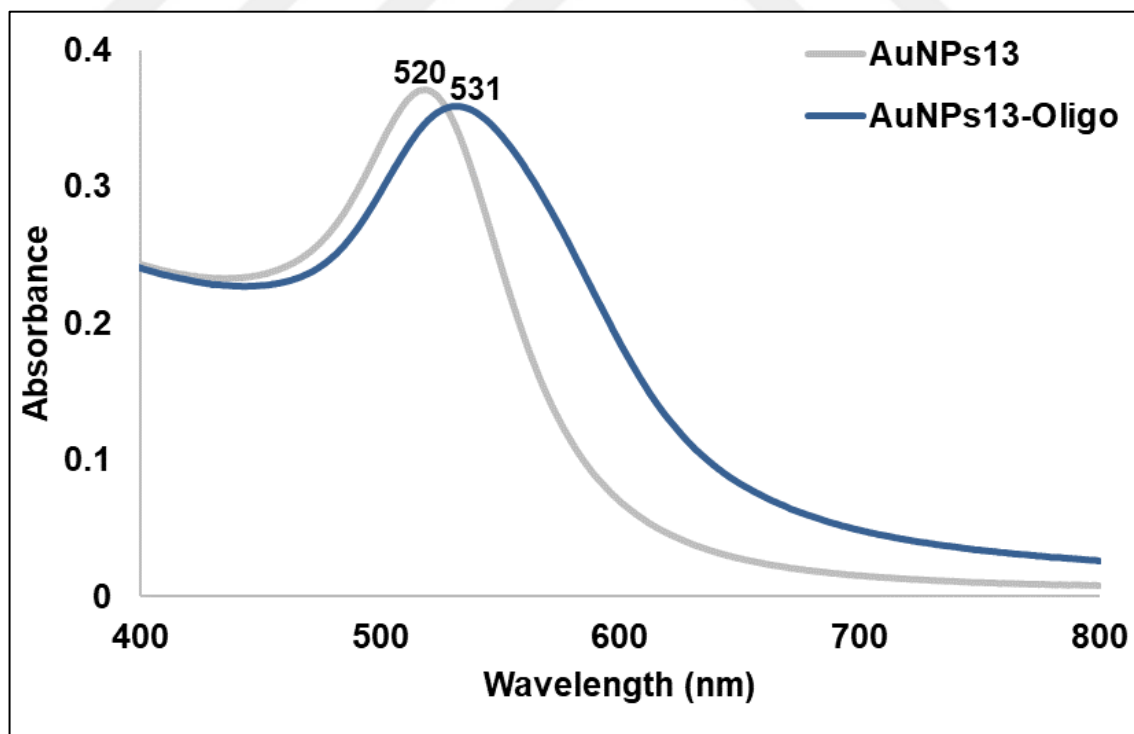
Figure 5.1. UV/Vis spectra of suspension of AuNPs13 and AuNPs13-Oligo.

The UV-Vis spectra of the AuNPs50 and AuNPs50-Oligo are shown in Figure 5.2. According to the literature, maximum wavelength for the AuNPs50 is at 532 nm [132]. When the AuNPs50 were modified with oligonucleotides, maximum wavelength shifted from 532 nm to 540 nm due to the modification and hydrodynamic size increase.
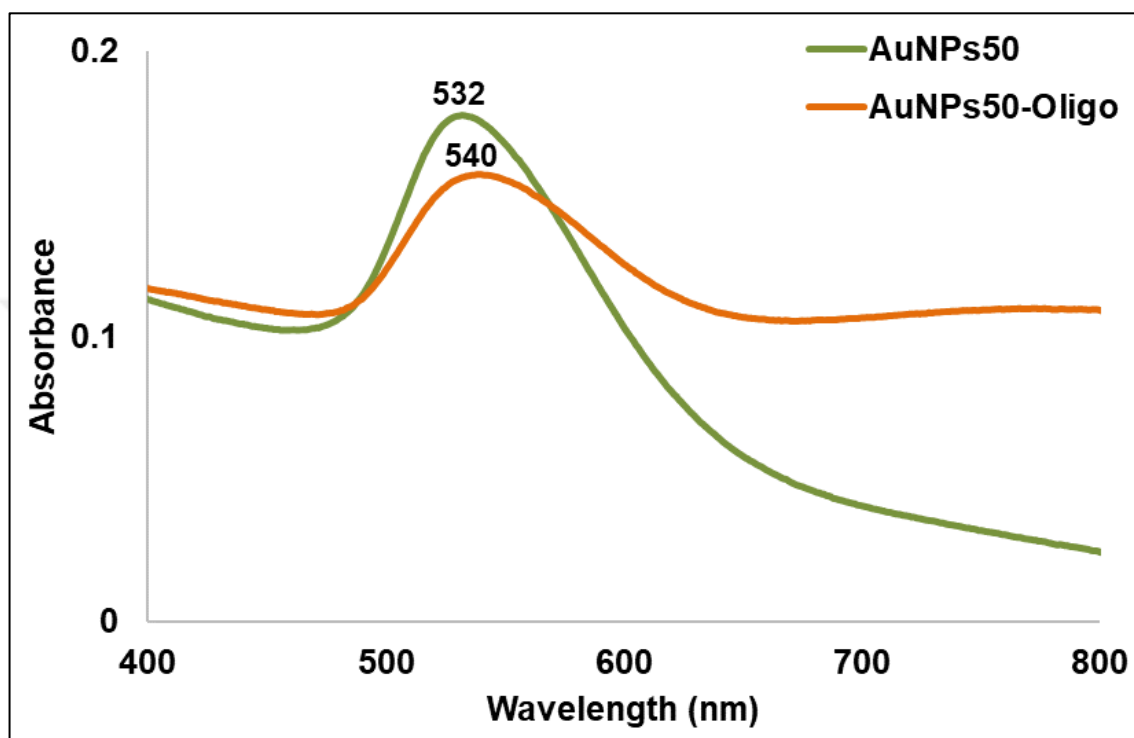
Figure 5.2. UV/Vis spectra of suspension of AuNPs50 and AuNPs50-Oligo.

5.1.2. Dynamic Light Scattering

Hydrodynamic sizes of AuNPs13 and AuNPs13-Oligo are shown in Figure 5.3. Hydrodynamic size of AuNPs13 is shifted from 13 to 28 when oligonucleotide modification was occurred.
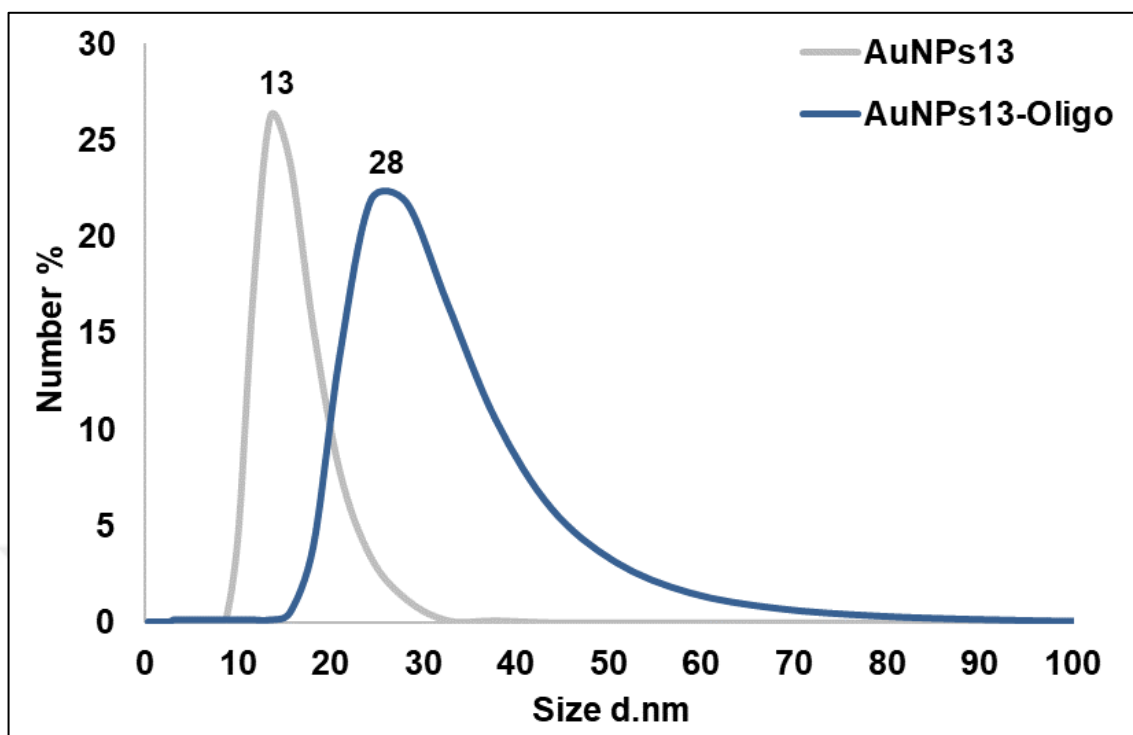
Figure 5.3. DLS spectra of suspension of AuNPs13 and AuNPs13-Oligo.

Hydrodynamic sizes of AuNPs50 and AuNPs50-Oligo are shown in Figure 5.4. Hydrodynamic size of AuNPs50 shifted from 58 to 90 when oligonucleotide modification was occurred.
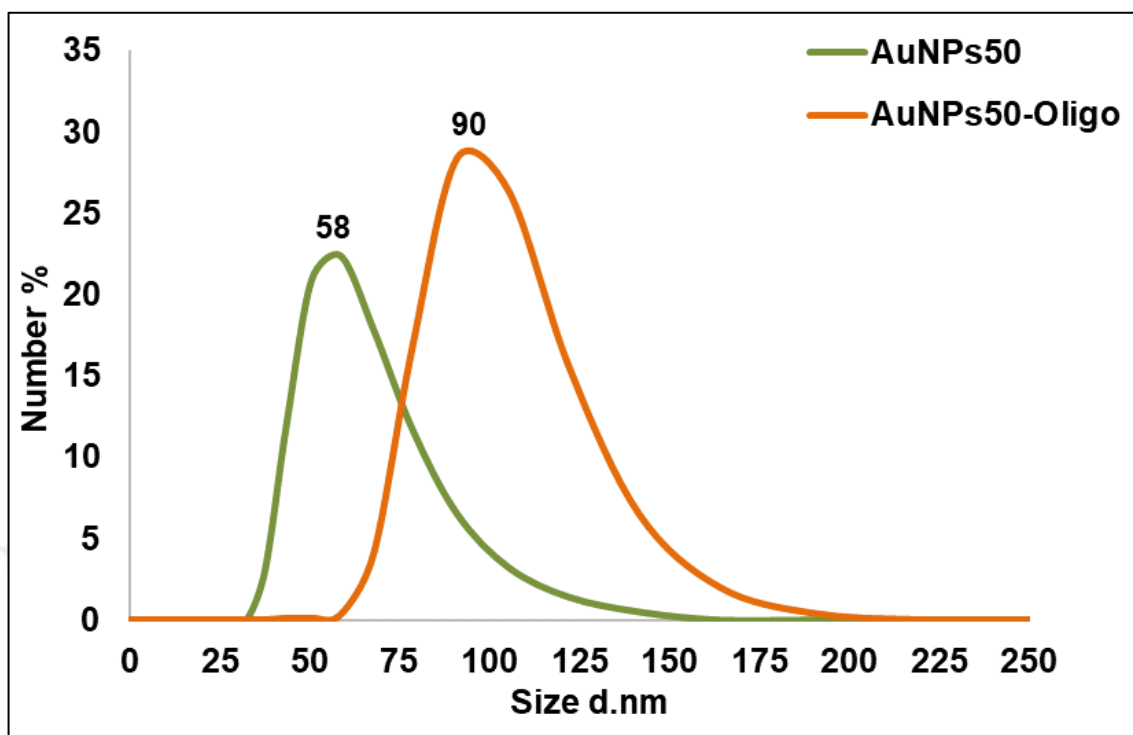
Figure 5.4. DLS spectra of suspension of AuNPs50 and AuNPs50-Oligo.

5.1.3. Transmission Electron Microscopy

TEM images of AuNPs13 and AuNPs50 are shown in Figure 5.5. Sizes of AuNPs13 and AuNPs50 are determined from TEM analysis to be about 13 nm and 50 nm, respectively.
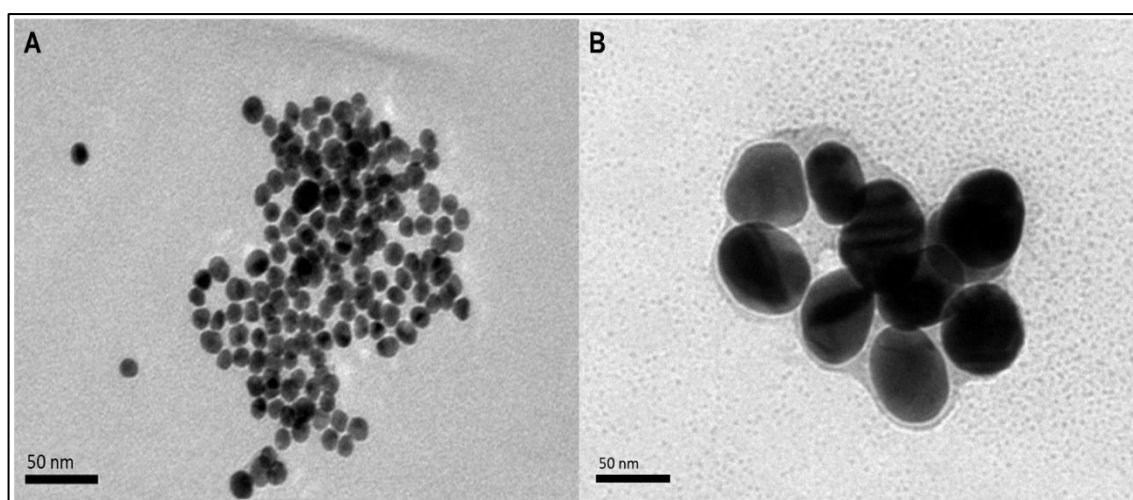
Figure 5.5. TEM images of the AuNPs with sizes of (a) 13 nm and (b) 50 nm.

5.2. WST-1 CELL VIABILITY ASSAY

It is known that AuNPs are non-toxic [85]. However, toxicity of AuNPs change depending on surface chemistry, shape, size, and aggregation status [87]. In this study, influences of AuNPs13, AuNPs13-Oligo, AuNPs50, AuNPs50-Oligo, mixture of AuNPs50 and AuNPs13, and mixture of AuNPs50 and AuNPs13-Oligo to cell viability were investigated. The cytotoxicity of AuNPs in the concentration of 2.5 nM to 20 nM was assessed and the results are shown in Figure 5.5.

According to the control group, AuNPs13, AuNPs13-Oligo, AuNPs50, AuNPs50-Oligo, and mixture of AuNPs50 + AuNPs13 did not show significant cytotoxic effect; 90 per cent cell viability was observed after 24 h treatment. However, cell viability decreased to 89 per cent when the cells were exposed to mixture of AuNPs50 + AuNPs13-Oligo at the concentration of 20 nM. The decrease in cell viability could be due to the aggregation status of AuNPs [133].
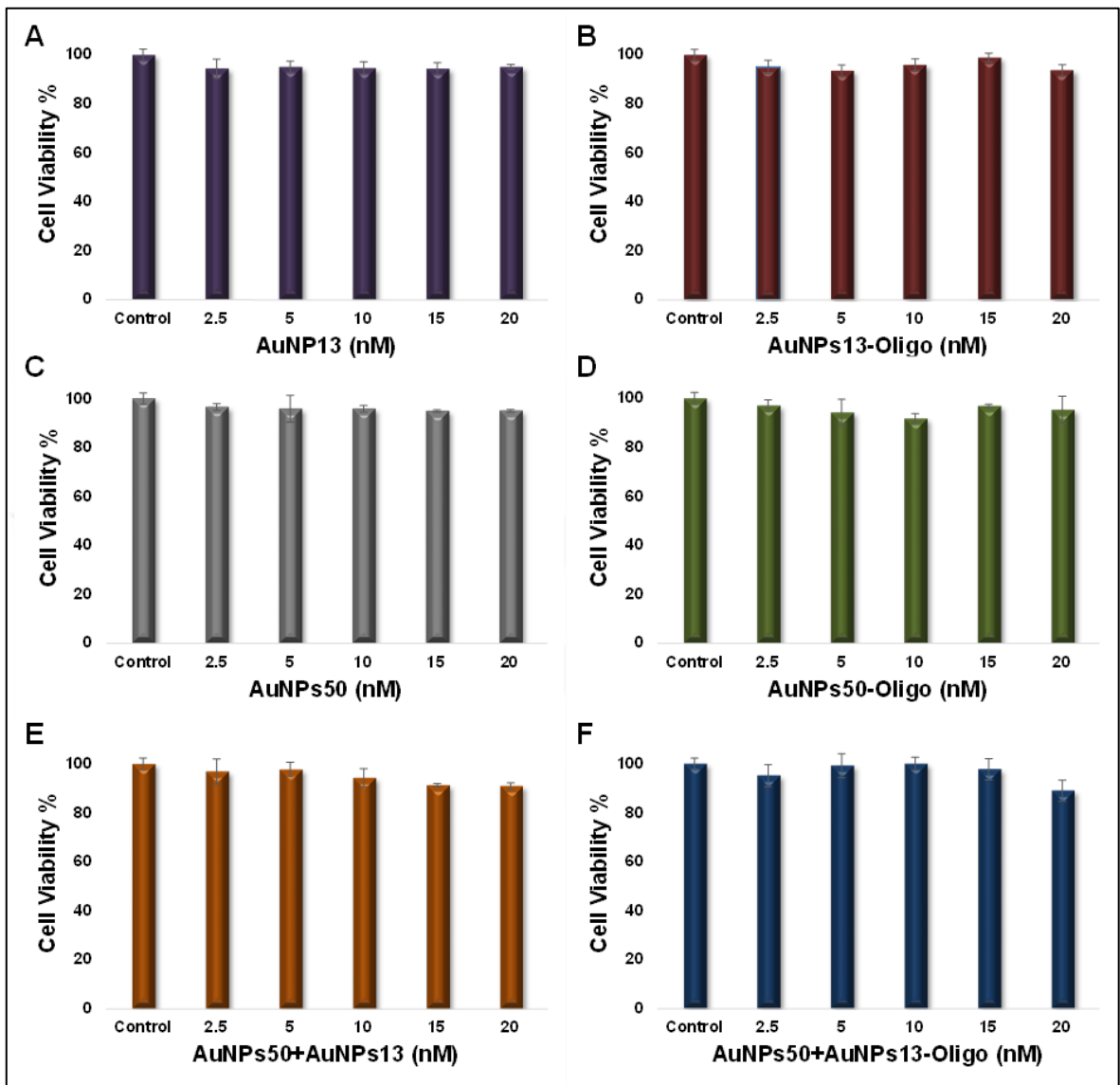
Figure 5.6. Cell viability of MDA-MB-231 cells treated at increasing concentrations of (a) AuNPs13, (b) AuNPs13-Oligo, (c) AuNPs50, (d) AuNPs50-Oligo. Mixture of (e) 25 nM of AuNPs50 and AuNPs13 with increasing concentration, and (f) 25 nM of AuNPs50 and AuNPs13-Oligo with increasing concentration.

5.3. SERS MEASUREMENT

The influence of surface chemistry difference on the uptake of AuNPs and molecular process taking place in single-cell were investigated using SERS. Cells were treated with 10 nM of AuNPs13, AuNPs13-Oligo, AuNPs50, AuNPs50-Oligo, mixture of AuNPs50 and AuNPs13, and mixture of AuNPs50 and AuNPs13-Oligo. After 4h, 8h, 12h, and 24h treatment, SERS spectra of the 20 MDA-MB-231 cells were collected. Intensities of SERS spectra and obtained spectral information from the cells changed depending the size, surface chemistry and the combinations of AuNPs mixtures, which were AuNPs13, AuNPs13-Oligo, AuNPs50, AuNPs50-Oligo, mixture of AuNPs50 and AuNPs13, and mixture of AuNPs50 and AuNPs13-Oligo has shown in Figure 5.6. AuNPs50 provided more intense spectra than the others due to the more efficiently uptake and intracellular aggregation while AuNPs13 and AuNPs13-Oligo did not show any SERS activity.
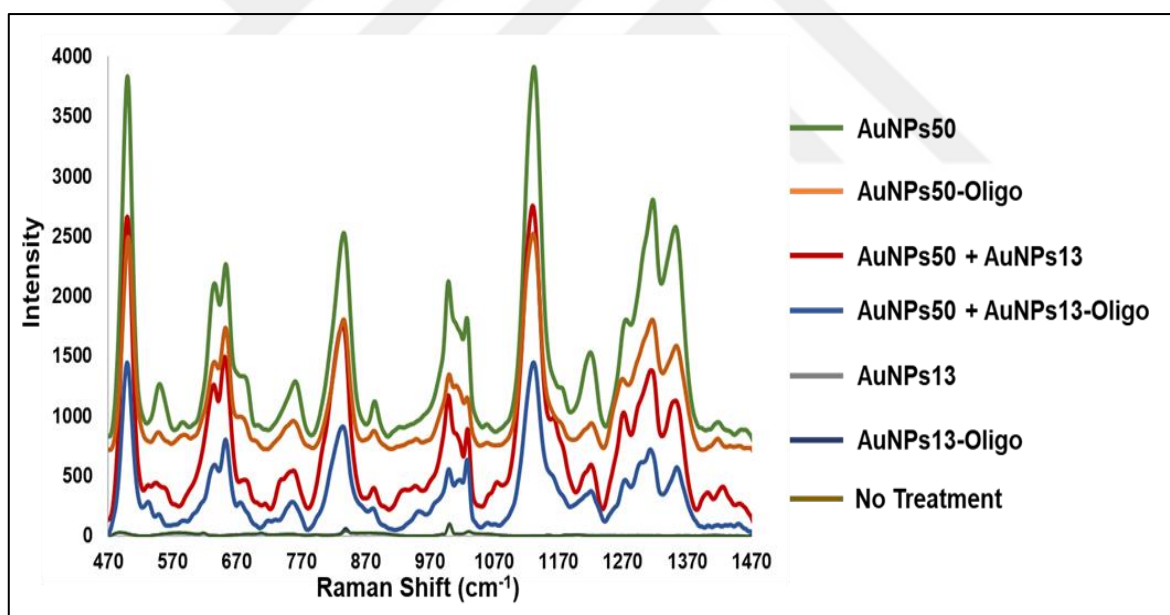
Figure 5.7. SERS spectra of MDA-MB-231 cells incubated with AuNPs50, AuNPs50-Oligo, AuNPs13, AuNPs13-Oligo, mixture of AuNPs50+ AuNPs13, and mixture of AuNPs50+ AuNPs13-Oligo for 24h.

To investigate possible spectral differences of AuNPs13 and AuNPs13-Oligo, SERS spectra of non-treated cells were also collected to check the spectral differences and the same spectra were obtained from the cells, shown in Figure 5.7. Thus, we can clearly say that AuNPs13 and AuNPs13-Oligo do not have any SERS activity up to 24 h exposure time.
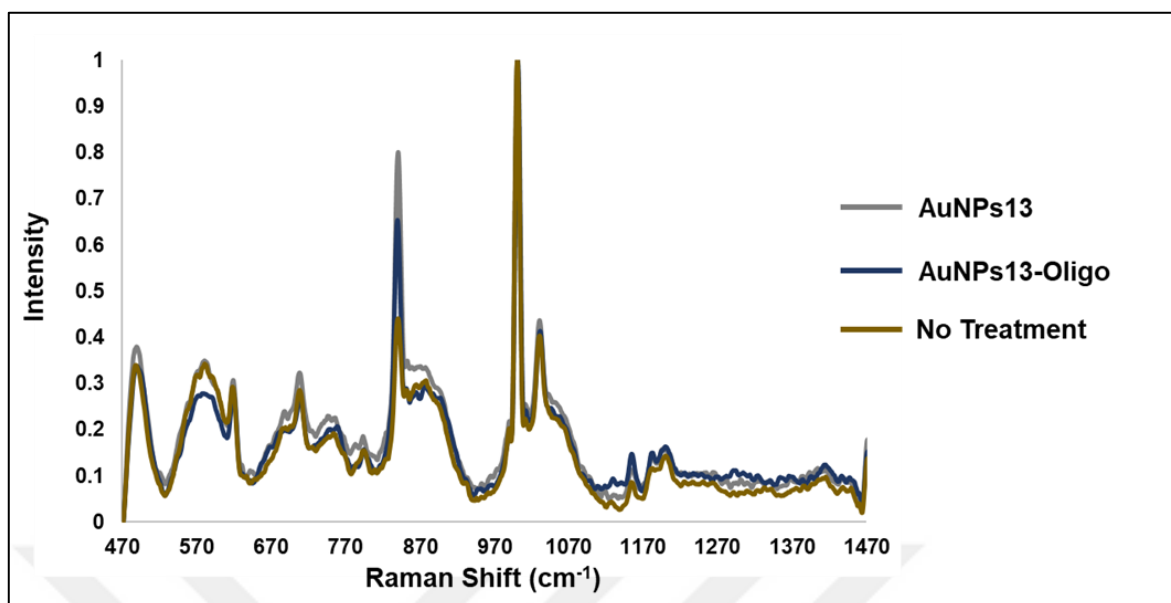
Figure 5.8. SERS spectra of MDA-MB-231 cells incubated with AuNPs13, AuNPs13-Oligo, and without incubation for 24h.

5.3.1. Time Dependent SERS Activity on AuNPs50

Time dependent SERS activity of AuNPs50 inside the cells was monitored after 4h, 8h, 12h, and 24h treatment. Firstly, cells were exposed to 10 nM of AuNPs50. An area of 20 cells were scanned after 4 h, 8 h, 12 h, and 24 h incubation. An average 36-64 spectra were collected from a single cell. The data of a single cell was pre-processed by applying subtract baseline, smoothing and normalization using Wire software.

The reproducibility of SERS spectra of the MDA-MB-231 cells treated with AuNPs50 obtained from each time point was shown in Figure 5.8. Coefficient of variation values (CV), which indicate the degree of variation of reproducibility of spectra from a group of single cells, were calculated for each group. As is seen in Figure 5.8., the reproducibility of spectra obtained at 4h and 8 h are very low while the reproducibility of spectra increased further incubation to 12 h and 24h. Dependently, CV values are observed as 75.62 per cent, 73.55 per cent, 53.21 per cent, and 38.34 per cent. The decrease in the CV values can indicate that the time-dependent uptake process of the cells and aggregation of AuNPs inside the cells. The small aggregates were started to comprise in the cells in 4 h. When the exposure time was increased, the uptake of AuNPs and their aggregation also increased because of the

particle aggregation in the vesicles or fusion of endosomes which contain nanoparticles. It was reported that formation of NPs aggregation depends on time [134].

Significant changes in peak intensities are clearly observed due to the molecular dynamics of the cells during exposure times. The average of spectra from 20 cells after 4h, 8h, 12h, 24h treatment is shown in Figure 5.8.(E). Briefly, the intensities at the 545 cm^{-1} (S-S), 640 cm^{-1} (C-C twisting of proteins), 646 cm^{-1} (C-C twisting mode of tyrosine), 662 cm^{-1} (C-S stretching mode of cystine), 687 cm^{-1} (C-N), 840 cm^{-1} (amine groups), 884 cm^{-1} (proteins), 1203 cm^{-1} (Amide III), 1223 cm^{-1} (cellular nucleic acids), 1278 cm^{-1} (Amide III), 1319 cm^{-1} (Amide III), 1337 cm^{-1} (Amide III), and 1420 cm^{-1} (nucleic acids) peaks which correspond to proteins and nucleic acids increased starting from 4 h to 24 h. The peaks at 717 cm^{-1} (membrane phospholipids), 813 cm^{-1} (phosphodiester bands), 1031 cm^{-1} (Phenylalanine), 1064 cm^{-1} (C-C stretch of lipids) and 1445 cm^{-1} (CH_2 deformation) which correspond to lipid also changed by decreasing the intensities from 4 h to 24 h [135-141].

These spectral changes reflect the inhomogeneity of a cell content and depending on localization and aggregation status of AuNPs50. For example, while the peak intensity at 717 cm^{-1} which corresponds to C-N bond in membrane phospholipids is decreased, the peak intensity at 884 cm^{-1} which corresponds to proteins is increased during exposure time. Because AuNPs50 could be still interacted with the cell membrane in 4 h or aggregation of AuNPs distributed nearly membrane. On the other hand, effect of membrane wrapping can be still remained in 4 h. After 12 h, AuNPs are uptaken into cells and larger aggregation started to occur near nucleus [142]. Therefore, peaks which correspond to protein, nucleic acids, RNA and DNA are increased while the exposure time is increased. The peaks between 1200 cm^{-1} - 1400 cm^{-1} indicates the amide III bonds which give structure information about the proteins. On the other hand, peak intensities at 1064 cm^{-1} and 1445 cm^{-1} decreased during 24 h because they indicate the C-C stretch and CH_2 deformation at lipids, respectively, which associated the membrane status. An another peak that corresponds to phosphodiester bond at 813 cm^{-1} also disappeared after 12 h. These spectral changes could indicate the motion of endosomes from early endosome to lysosomes.

Spectral changes at 545 cm^{-1}, 640 cm^{-1}, 646 cm^{-1} and 687 cm^{-1} which correspond to S-S and C-C bonds of proteins were clearly observed after 8 h. This situation indicates the endosome maturation. Since early endosomes link to lysosomes or form the fusion

endosomes, proteins take very important role. Thus, the spectral changes can be explained as endosome maturation process after 8 h.

Figure 5.9. Reproducibility of SERS spectra of 20 MDA-MB231 cells incubated with AuNPs50 for (a) 4 h, (b) 8 h, (c) 12 h, (d) 24 h. (e) Comparison of average of SERS spectra obtained from different incubation times.

5.3.2. Time Dependent SERS Activity On AuNPs50-Oligo

Time dependent SERS activity was monitored after 4 h, 8 h, 12 h, and 24 h AuNPs50-Oligo treatment. The reproducibility of SERS spectra obtained from each time point was shown in Figure 5.9. CV values were calculated for each group. As expected, the reproducibility of spectra was increased from 4 h to 24 h. Dependently, the CV values are observed as 55.81 per cent, 51.81 per cent, 49.15 per cent, and 42.29 per cent. CV values of AuNPs50-Oligo uptake at 4 h, 8 h, and 12 h are smaller than AuNPs50 uptake. These results could be explained with the time dependent intracellular uptake efficiency and the aggregation. AuNPs-Oligo could enter the cells more efficiently than AuNPs or localization of AuNPs50-Oligo have differences from AuNPs50 treatment [143]. However, CV value of AuNPs50-Oligo treatment was more than CV value of AuNPs50 treatment at 24 h. It could be caused by the particle loss due to exocytosis [142].

Intensities at the 552 cm^{-1} (S-S), 585 cm^{-1} (S-S), 678 cm^{-1} (Ring breathing modes in the DNA bases), 1228 cm^{-1} (Amide III), 1275 cm^{-1}(Amide III), 1317 cm^{-1}(Amide III), 1420 cm^{-1} (nucleic acids) peaks which correspond to nucleic acids and proteins also increased during the treatment of AuNPs50-Oligo and the peaks at 620 cm^{-1} (C-C twist), 729 cm^{-1} (Adenine), 960 cm^{-1} (vibration of PO_4), and 1064 cm^{-1} (C-C stretch of lipids) which correspond to lipids also decreased [137, 138, 140, 141]. The peak intensity at 717 cm^{-1} which corresponds to C-N bond in membrane phospholipids decreased for 8 h and 24 h treatment.

For example, there is a significant decrease at 960 cm^{-1} and 1064 cm^{-1} after 4 h which correspond to PO_4 and C-C in lipids, respectively. And at 1228 cm^{-1} which correspond to amide III sharpened during increased exposure time. Also the peaks between 1200 cm^{-1} and 1400 cm^{-1} indicates the amid III bonds which give structure information about the proteins increased during exposure time. Between 500 cm^{-1} and 600 cm^{-1} which correspond to S-S bond, spectral changes are observed during the protein interaction. The peak intensity at 729 cm^{-1} which corresponds to Adenine disappeared after 4 h. This peak could be caused by the poly-Adenine oligonucleotides. The peak at 1420 cm^{-1}, attributed nucleic acids, showed up after 8 h. As we expected, the spectral changes which correspond to protein, lipids and nucleic acids are observed and generally the intensities of protein and nucleic acid peaks increased and the lipid peaks decreased since the exposure time increased.
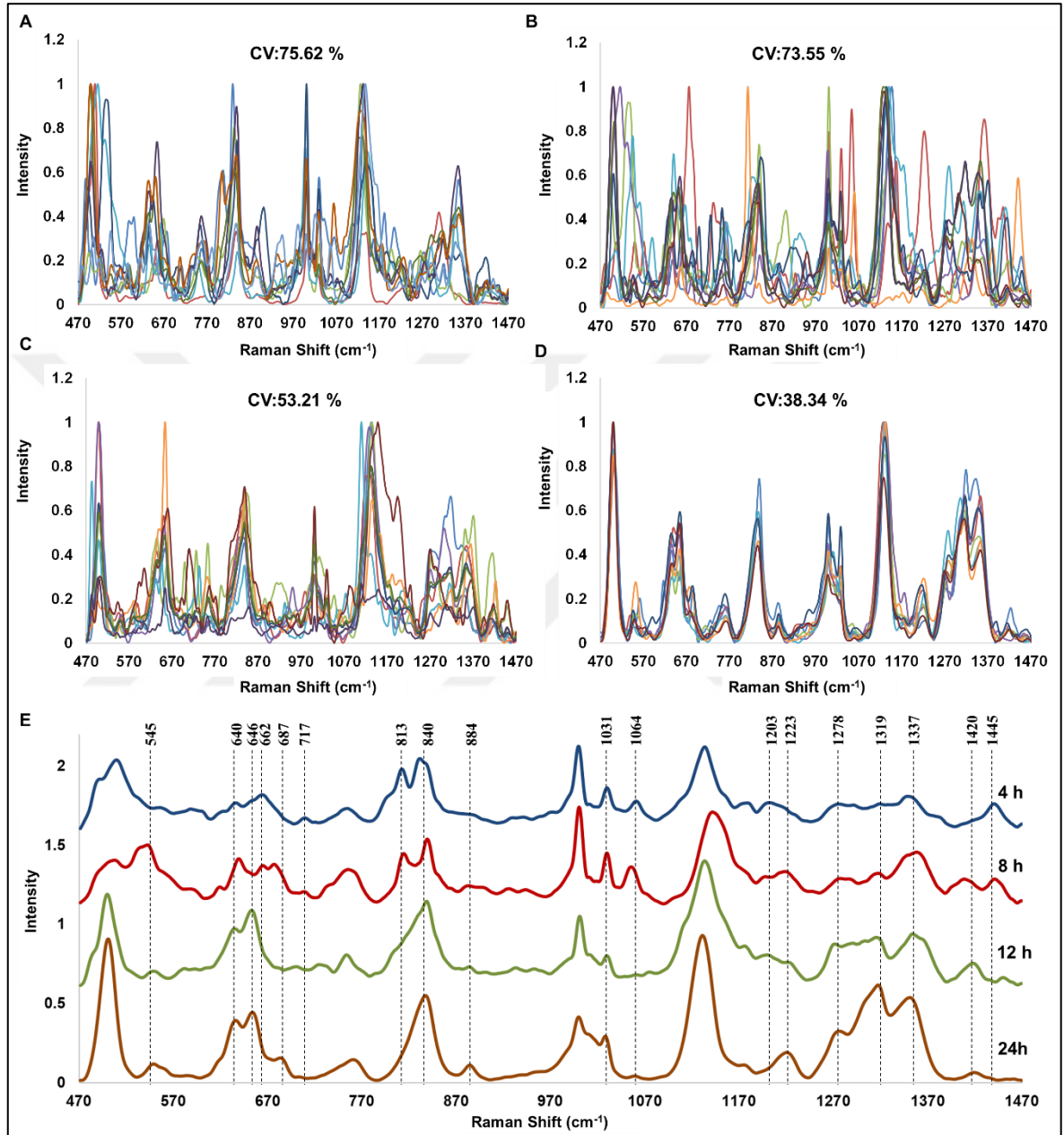
Figure 5.10. Reproducibility of SERS spectra of 20 MDA-MB231 cells incubated with AuNPs50-Oligo for (a) 4 h, (b) 8 h, (c) 12 h, (d) 24 h. (e) Comparison of average of SERS spectra obtained from different incubation times.

5.3.3. Time Dependent SERS Activity on Mixture of AuNPs50 + AuNPs13

Beside the effects of surface chemistry of AuNPs, effects of intracellular aggregation status of AuNPs to SERS spectra were investigated. The particle size of nanoparticles influences the nanoparticle uptake and intracellular aggregation status. However, the efficiency of internalization of difference sizes of nanoparticles when they are exposed together is unknown. Although not yet certain, influence of uptake and intracellular aggregation status of different sizes on SERS enhancement was investigated using mixture of AuNPs50 and AuNPs13 in this study.

AuNPs50 were added to the medium in 25 percent (v/v) of 1 mL which was the optimal amount for the SERS enhancement [113]. 10 nM of AuNPs13 were added to same incubation medium and MDA-MB-231 cells were incubated with mixture of AuNPs50 and AuNPs13 for 4 h, 8 h, 12 h, and 24 h.

Time dependent SERS activity was monitored after 4 h, 8 h, 12 h and 24 h mixture of AuNPs50 and AuNPs13 treatment. The reproducibility of SERS spectra obtained from each time point was shown in Figure 5.10. CV values were calculated for each group. As expected, the reproducibility of spectra is increased from 4 h to 24 h. Dependently, the CV values are observed as 61.05 per cent, 60.99 per cent, 58.72 per cent, and 41.60. CV values of AuNPs50 + AuNPs13 uptake at 4 h, 8 h, and 12 h are smaller than AuNPs50 uptake. It could be explained by the aggregation status of AuNPs50 and AuNPs13 during the uptake process and eventually in the cells.

Intensities at the 555 cm^{-1} (S-S), 646 cm^{-1} (C-C twisting mode of tyrosine), 678 cm^{-1} (Ring breathing modes in the DNA bases), 884 cm^{-1}(Proteins), 1275 cm^{-1} (Amide III), and 1302 cm^{-1} (Amide III) peaks which correspond to nucleic acids and proteins increased during the treatment and the peaks at 717 cm^{-1} (membrane phospholipids) and 960 cm^{-1} (stretching vibration of PO$_4$) which correspond to lipids decreased [137, 138, 140, 141, 144].

Spectral changes are observed between 500 cm^{-1} and 600 cm^{-1} correspond to S-S bond for 4 h and 8 h. It could be explained as motion of endosomes in the cell. During the motion, proteins such as kinesin, dynein take role thus peaks that correspond to proteins exhibited intensity changes during exposure time. For example, significant increase was observed at 646 cm^{-1} which correspond to C-C twisting mode of tyrosine. While the peaks at 717 cm^{-1}

and 960 cm^{-1} which correspond to C-N and PO$_4$ at lipids disappear after 24 h. As we expected, CV value was decreased during exposure time and protein peaks increased while the lipid peaks decreased. As is seen in Figure 5.8, Figure 5.9, and Figure 5.10 number of spectral changes are less than the AuNPs50 and AuNPs50-Oligo treatment. It could be caused by aggregation status of AuNPs in the lysosomes which means the end of the endocytosis pathway.
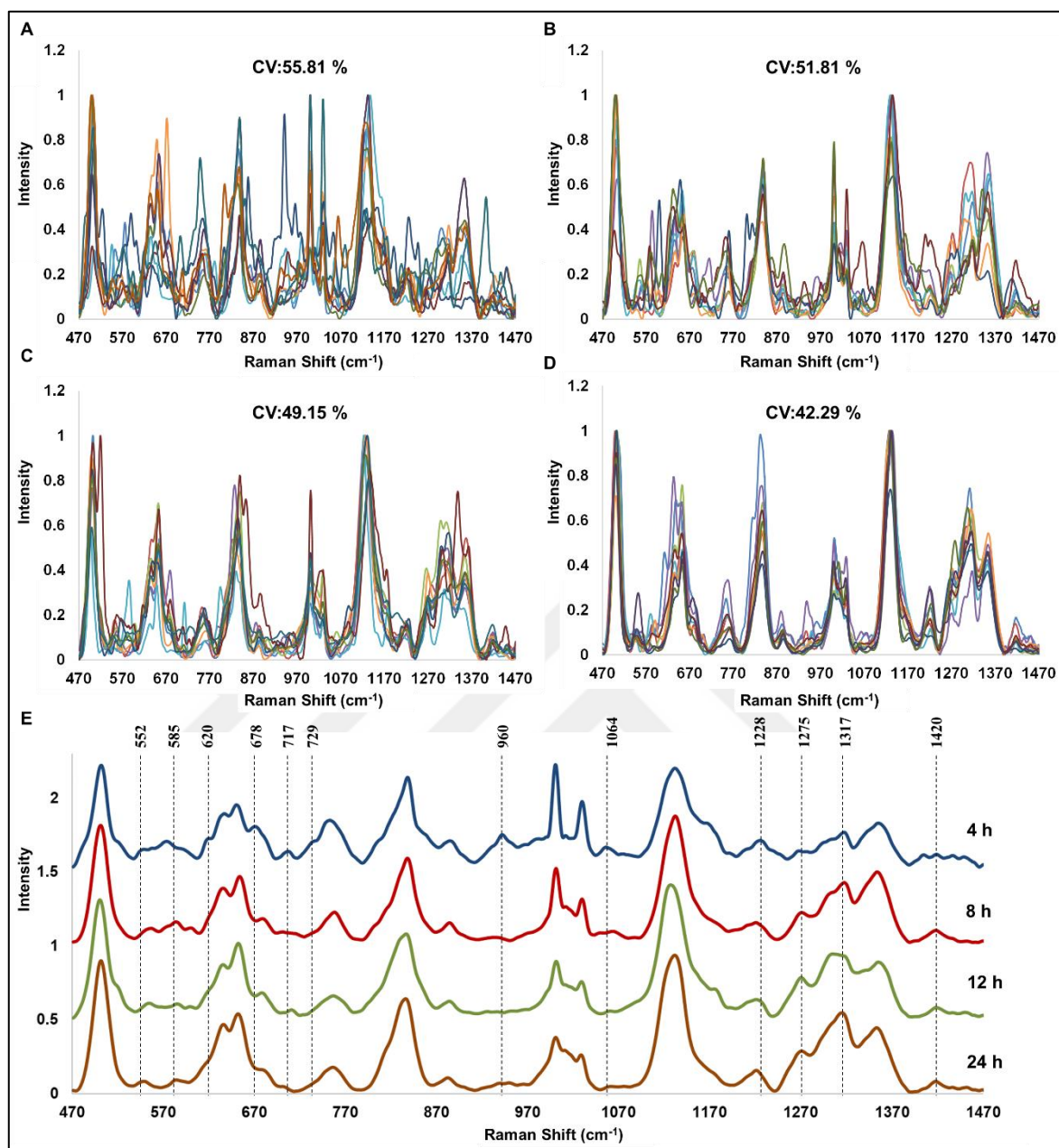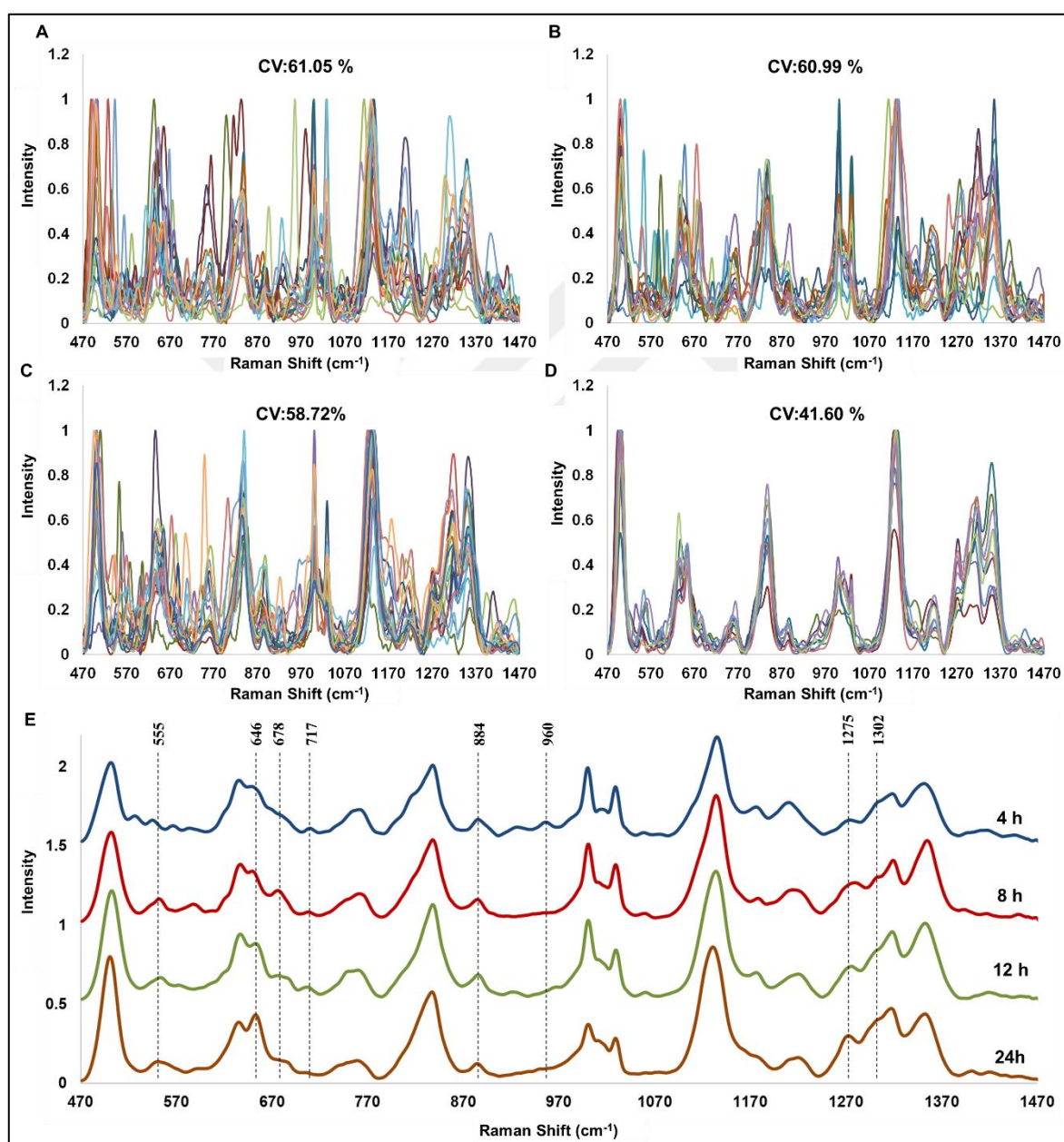

Figure 5.11. Reproducibility of SERS spectra of 20 MDA-MB-231 cells incubated mixture of AuNPs50 and AuNPs13 for (a) 4 h, (b) 8 h, (c) 12 h, (d) 24 h. (e) Comparison of average of SERS spectra obtained from different incubation times.

5.3.4. Time Dependent SERS Activity on Mixture of AuNPs50 + AuNPs13-Oligo

While the particle size of nanoparticles influences the nanoparticle uptake and intracellular aggregation status, surface chemistry of AuNPs also influences the aggregation status. Therefore, AuNPs13-Oligo was used in mixture to investigate the influence of surface chemistry to SERS spectra.

AuNPs50 were added to the medium in 25 percent (v/v) of 1 mL and 10 nM of AuNPs13-Oligo were added to same incubation medium and MDA-MB-231 cells were incubated with mixture of AuNPs50 and AuNPs13-Oligo for 4 h, 8 h, 12 h, and 24 h

Time dependent SERS activity was monitored after 4 h, 8 h, 12 h, and 24 h mixture of AuNPs50 and AuNPs13-Oligo treatment. The reproducibility of SERS spectra obtained from each time point was shown in Figure 5.11. CV values were calculated for each group. As expected, the reproducibility of spectra is increased from 4 h to 24 h. Dependently, the CV values are observed as 63.19 per cent, 62.81 per cent, 57.46 per cent, and 53.09. CV values of mixture of AuNPs50 + AuNPs13-Oligo treatment at 4h, 8h, and 24h are larger than AuNPs50+AuNPs13 treatment. It could be caused by the size increase of AuNPs50 and AuNPs13-Oligo compared to AuNPs50 +AuNPs13.

Intensities at the 548 cm^{-1} (S-S), 646 cm^{-1} (C-C twisting mode of tyrosine), 678 cm^{-1} (Ring breathing modes in the DNA bases), 760 cm^{-1} (Ring breathing tryptophan), 884 cm^{-1} (Proteins), 1224 cm^{-1} (Amide III), 1247 cm^{-1} (Amide III), and 1260 cm^{-1}(Amide III), peaks which correspond to nucleic acids and proteins increased during the treatment and the peak at 717 cm^{-1} (membrane phospholipids) and 800 cm^{-1} (phosphate ion interactions) which correspond to lipids decreased [136, 137, 140, 141, 144-146].

The peak at 646 cm^{-1} which corresponds to C-C twisting mode of tyrosine significantly increased while the peak at 800 cm^{-1} corresponds to phosphate ion interactions significantly decreased after 24 h. 1224 cm^{-1}, 1247 cm^{-1}, and 1260 cm^{-1} corresponds to Amide III increased during exposure time.

On the other hand, it can be said that to monitor the changes in the cells, mixture of AuNPs50 and AuNPs13-Oligo is more suitable than mixture of AuNPs50 and AuNPs13. As is seen

form figure 5.11, we can clearly observe the protein and lipid changes during exposure time for mixture of AuNPs50 and AuNPs13-Oligo treatment.
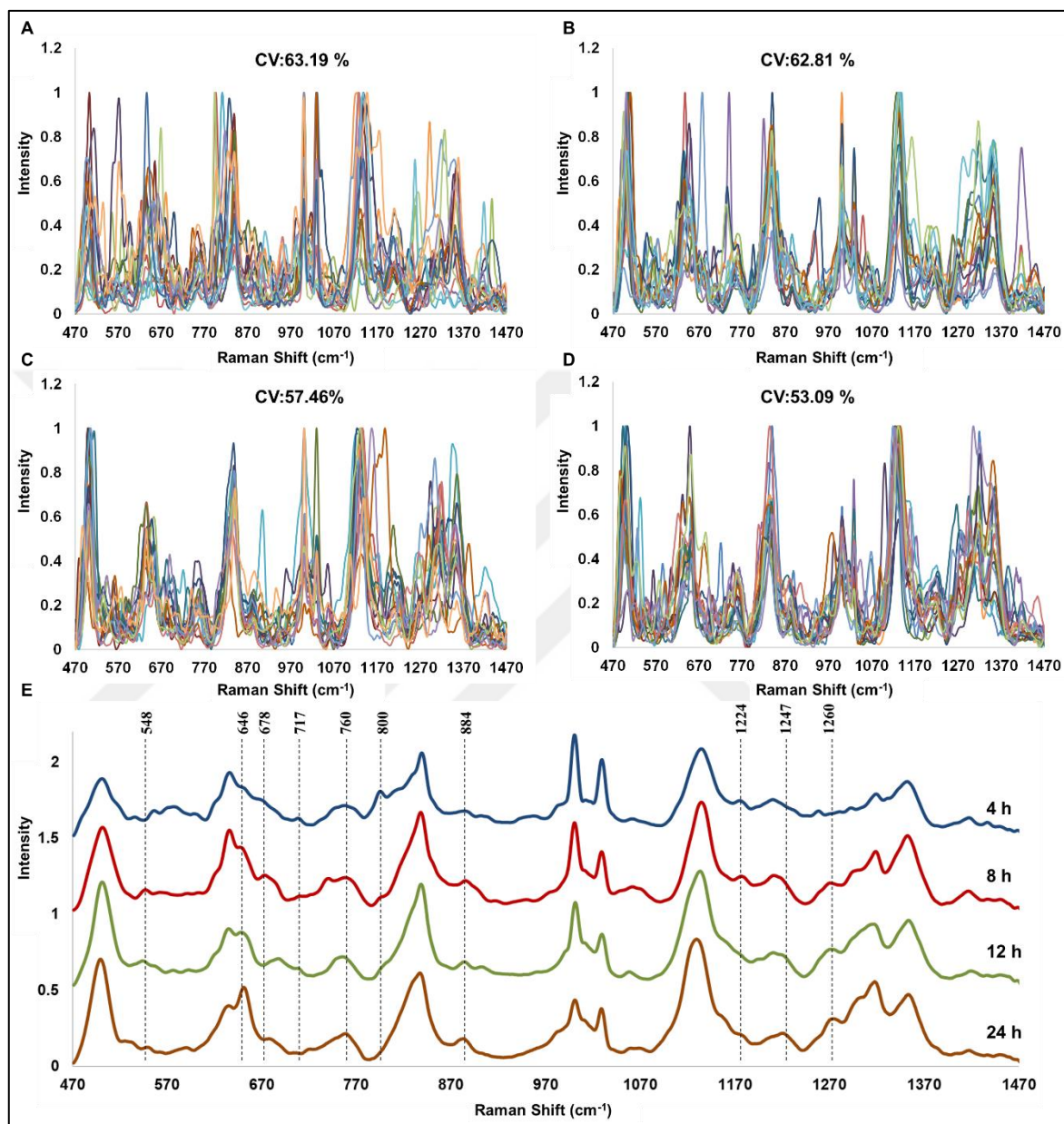
Figure 5.12. Reproducibility of SERS spectra of 20 MDA-MB231 cells incubated mixture of AuNPs50 and AuNPs13-Oligo for (a) 4 h, (b) 8 h, (c) 12 h, (d) 24 h. (e) Comparison of average of SERS spectra obtained from different incubation times.

According to the time dependent SERS activity measurement, it was observed that the SERS spectra of 24 h treatment was more reproducible than 4 h, 8 h, and 12 h treatment. It could be inferred from the spectral changes of all treatments, peaks which correspond to proteins increased while the lipid decreased during the endosomal activity depends on time.

5.3.5. SERS Activity on AuNPs After 4 h Treatment

According to the comparison of the time-dependent spectra it can be said that AuNPs50, AuNPs50-Oligo, mixture of AuNPs50 + AuNPs13 and mixture of AuNPs50 + AuNPs13-Oligo were uptaken and aggregation status changed during exposure time. However, to understand the effects of size and surface chemistry, the SERS spectra of different AuNPs treatments should be compared at the same exposure time.

It was expected to measure the correlation between the size, surface chemistry and aggregation status of nanoparticle and the SERS spectra obtained from cells during endocytosis process. Thus, we expect the monitor the molecular changes.

The averaged spectrum of the cells were compared according to the particle treatment in same incubation time. The spectral changes of the cells which were treated for 4 h are shown in Figure 5.12. Intensity changes of the peaks at 552 cm^{-1} (S-S), 640 cm^{-1} (C-C twisting of proteins), 662 cm^{-1} (C-S stretching mode of cystine), 755 cm^{-1} (Symmetric breathing of tryptophan), 890 cm^{-1} (Protein bands), 1172 cm^{-1} (tyrosine), 1224 cm^{-1}(Amide III), 1269 cm^{-1} (Amide III), 1296 cm^{-1} (Amide III), and 1230 cm^{-1} (Amide III) which correspond to proteins and nucleic acids; the peaks at 576 cm^{-1} (Phosphatidylinositol), 717 cm^{-1}(membrane phospholipids), 800 cm^{-1} (phosphate ion interactions), 1064 cm^{-1} (C-C stretch of lipids), and 1445 cm^{-1} (CH$_2$ deformation) which correspond to lipids and phosphates were observed.

As is seen from the Figure 5.12., so many spectral changes were observed after 4 h treatment because of the aggregation status and endocytosis process. Clathrin-mediated endocytosis is utilized to uptake of AuNPs smaller than 200 nm [14]. Protein–protein or protein–lipid interactions take important roles in the coat nucleation and assembly [147]. Thus, spectral changes generally correspond to proteins and lipids.

For endocytosis, firstly membrane wrapping is occurred [147]. Thus, in 4 h , the spectral changes correspond to protein and lipids were expected during membrane wrapping and vesicle forming. For example, peak intensities at 640 cm^{-1}, 662 cm^{-1} , and 755 cm^{-1} which correspond to proteins are increased and also peaks between 1200 cm^{-1} - 1400 cm^{-1} which correspond to Amide III for proteins increased for AuNPs-50-Oligo. Because proteins take important role to form the vesicles after membrane wrapping. Therefore, it could be said that

while AuNPs can be still interacted with cell membrane, the endosomal vesicles were started to be formed during AuNPs50-Oligo treatment in 4 h. These spectal changes were also observed for the treatment of AuNPs50 + AuNPs13-Oligo mixture. So, effects of oligonucleotides on cellular uptake and endocytic process could be observed during 4 h.

In addition to these, the peak at 1445 cm^{-1} which corresponds to CH$_2$ deformation and the peak at 1064 cm^{-1} which corresponds to C-C bond in lipids were observed for AuNPs50 while the peaks at 552 cm^{-1}, 1172 cm^{-1} and 890 cm^{-1} which correspond to nucleic acids and proteins were observed for just AuNPs50-Oligo. These spectral changes can enable us to understand the biochemical changes during uptake and regulation of different surface chemistry of nanoparticles in the cells.

On the other hand, the peak at 800 cm^{-1} which corresponds to phosphate can be representative of ATP. Since motion of endosomes started, ATP takes very important role for the motion and pH regulation in the cells. The result indicates that molecules might have been carried with gold nanoparticle inside the cell.

Molecules around the AuNPs in the cells change thus spectral changes were observed. Therefore, the SERS spectra enables us to understand the molecular environmental change such as the presence or absence of transport proteins. On the other hand, endosomes are motile and their movements linked to their stage of function and maturation. The movement is mediated by both kinesin and dynein motor proteins. Thus, spectral changes were observed for the proteins and lipids.

Figure 5.13. SERS spectra of MDA-MB-231 cells incubated with AuNPs50, AuNPs50-Oligo, mixture of AuNPs50+ AuNPs13, and mixture of AuNPs50+ AuNPs13-Oligo for 4h.

5.3.6. SERS Activity on AuNPs After 8 h Treatment

The averaged spectrum of the cells were compared according to the particle treatment in same incubation time. The spectral changes of the cells which were treated for 8h are shown in Figure 5.13.. Intensity changes of the peaks at 560 cm^{-1} (S-S), 589 cm^{-1} (PO$_4$), 640 cm^{-1} (C-C twisting of proteins), 656 cm^{-1} (Guanine), 682 cm^{-1} (C-S), 717 cm^{-1} (membrane phospholipids), 733 cm^{-1} (phosphatidylserine), 890 cm^{-1} (protein bands), 1064 cm^{-1} (C-C stretch of lipids), 1224 cm^{-1} (Amide III), 1260 cm^{-1} (Amide III), 1320 cm^{-1} (Amide III), and 1420 cm^{-1} (nucleic acids) were observed.

After 8 h treatment, spectral changes especially between 500 cm^{-1} and 600 cm^{-1} which correspond to proteins and nucleic acids are observed. This can be explained that after 8 h, endosomes start to form the multivescilar bodies which is also called formation of late endosomes. Various proteins and receptors take role for the endosome maturation. Since endosomes are not in close proximity to cell membrane, there are not any spectra changes correspond to lipids expect the peak at 1064 cm^{-1} which corresponds to C-C stretch of lipids. This peak is observed for AuNPs50 treatment only. Some of the aggregation of AuNPs50 still could be remained close to membrane during 8 h.

It is difficult to link the detected spectra and the molecular basis of transport. However, phosphate signal could be representative of ATP and it could be caused by the start of increased motion or change in motion direction since ATP controlled the motion. Thus, the peak at 733 cm^{-1} which corresponds to phosphatidylserine can be explained for mixture of AuNPs50 + AuNPs13-Oligo treatment.

On the other hand , the peak intensity at 890 cm^{-1} corresponds to protein bands is observed for the AuNPs50-Oligo and mixture of AuNPs50 + AuNPs13-Oligo treatments and also increase in protein peak intensities for AuNPs50-Oligo and mixture of AuNPs50 + AuNPs13-Oligo were observed. Thus, it can be said that effects of oligonucleotides to cellular uptake and endocytosis process can be observed using SERS also in 8 h.

Figure 5.14. SERS spectra of MDA-MB-231 cells incubated with AuNPs50, AuNPs50-Oligo, mixture of AuNPs50+ AuNPs13, and mixture of AuNPs50+ AuNPs13-Oligo for 8h

5.3.7. SERS Activity on AuNPs After 12 h Treatment

The averaged spectrum of the cells were compared according to the particle treatment in same incubation time. The spectral changes of the cells which were treated for 12 h are shown in Figure 5.14. Intensity changes of the peaks at 555 cm^{-1} (S-S), 589 cm^{-1} (PO$_4$), 640 cm^{-1} (C-C twisting of proteins), 728 cm^{-1} (C-C, proline), 1265 cm^{-1} (Amide III), 1275 cm$^-$

[1](Amide III), 1302 cm[-1](Amide III), 1356 cm^{-1} (Guanine) and 1420 cm^{-1} (nucleic acids) were observed.

After 12 h treatment, the number of spectral changes started to decrease during the endosome maturation. Since the environment of AuNPs changed the spectra of the cells after 12 h also change. The spectral changes are observed at 555 cm^{-1}, 589 cm^{-1}, 640 cm^{-1} and 728 cm^{-1} which correspond to S-S and C-C bond in proteins, respectively.

For 12 h treatment, the peak at 1420 cm^{-1} show high intensity for AuNPs50. When pH is between 6.2 and 6.9, COO[-] released and the peak assignment is observed at 1420 cm^{-1}. However, this situation is for the early endosome or just before the late endosome [148]. Although not yet certain, AuNPs50 could be still remained at early endosomes or near the cell membrane after 12 h .
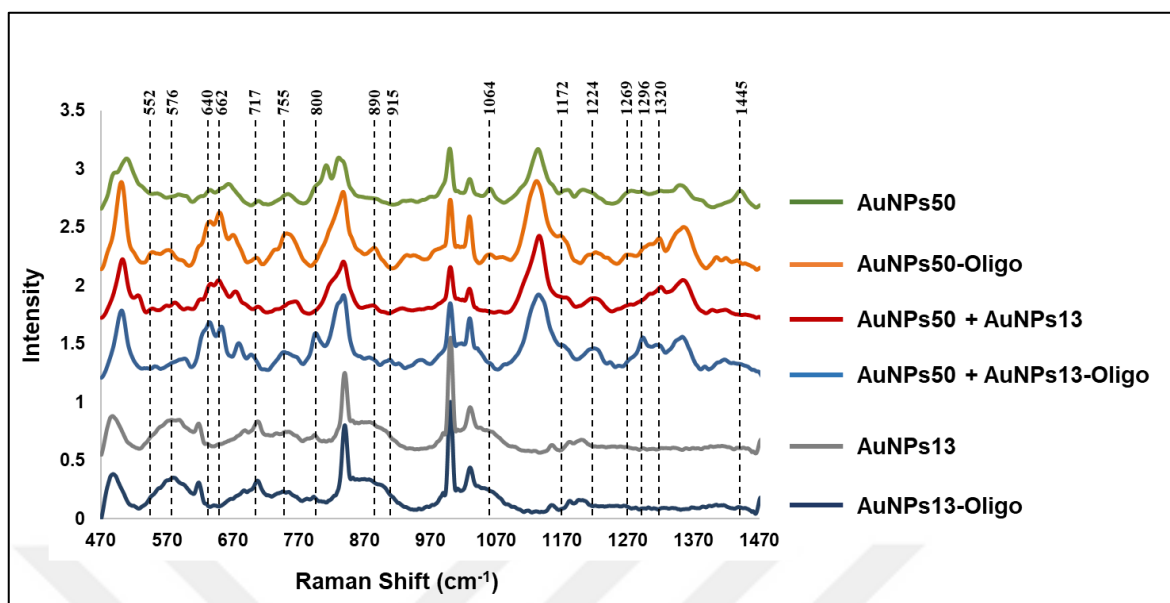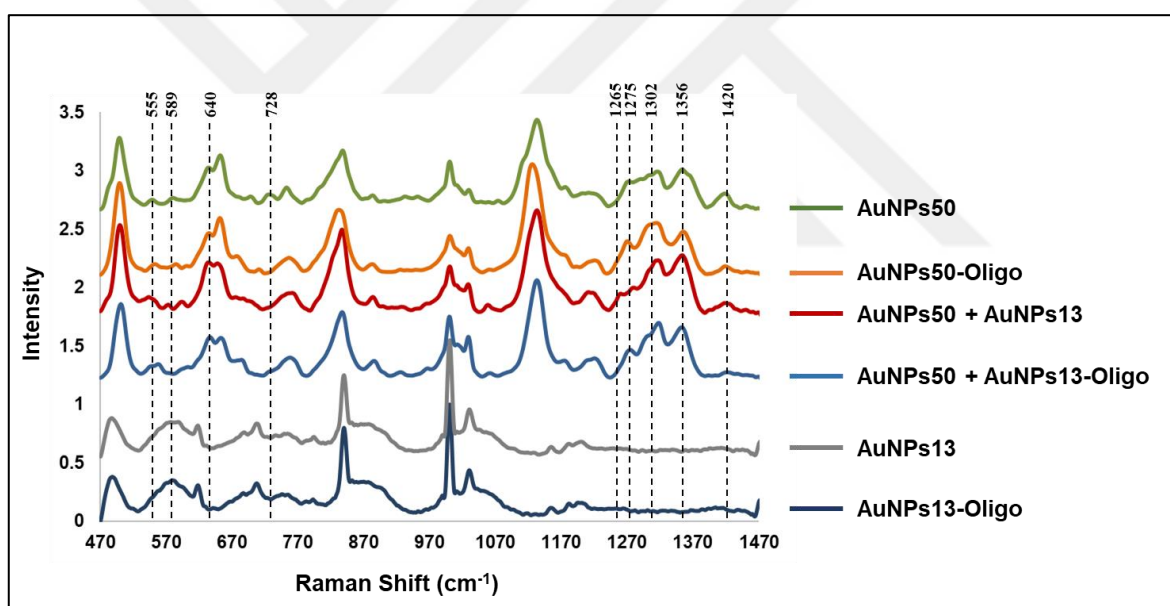

Figure 5.15. SERS spectra of MDA-MB-231 cells incubated with AuNPs50, AuNPs50-Oligo, mixture of AuNPs50+ AuNPs13, and mixture of AuNPs50+ AuNPs13-Oligo for 12h.

5.3.8. SERS Activity on AuNPs After 24 h Treatment

The averaged spectrum of the cells were compared according to the particle treatment in same incubation time. The spectral changes of the cells which were treated for 24 h were shown in Figure 5.15. Intensity changes of the peaks at 552 cm^{-1} (S-S) , 589 cm^{-1} (PO$_4$), 689 cm^{-1} (C-N), 725 cm^{-1} (Adenine), and 1298 cm^{-1} (Amide III) were observed.

After 24 h treatment, the number of spectral changes are significantly decreased because of the aggregation status and endosomal process. As we expected, uptake of AuNPs should be completed after 24 h. The spectral changes between 552 cm^{-1} and 725 cm^{-1} correspond to Adenine and Phosphate can be occurred during the VATPases which is responsible for acidification during endocytosis or enhancement of phosphate peak can be caused by the aggregation in lysosomes [149]. Phosphate resulting from the digestion and turnover of nucleic acids is found in lysosomes which are known accumulation points of nanoparticles.
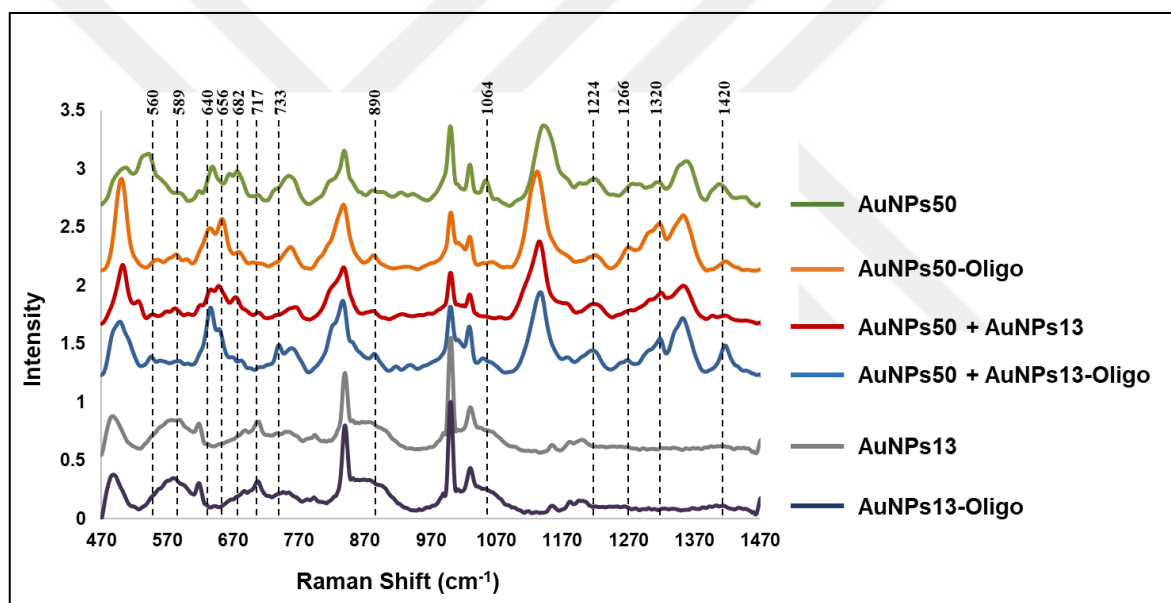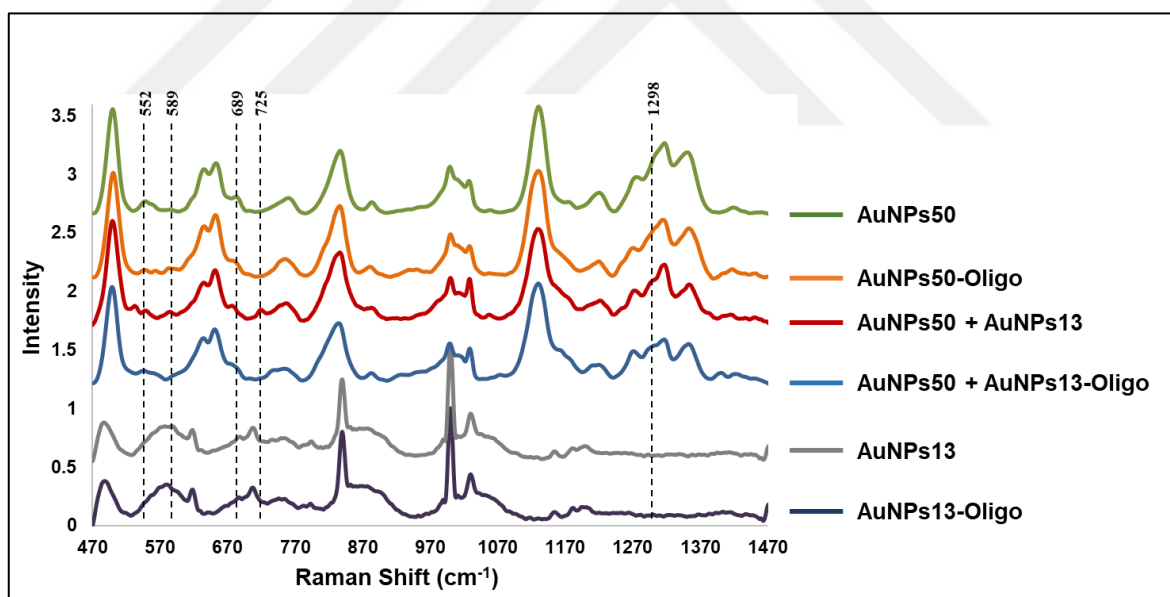

Figure 5.16. SERS spectra of MDA-MB-231 cells incubated with AuNPs50, AuNPs50-Oligo, mixture of AuNPs50+ AuNPs13, and mixture of AuNPs50+ AuNPs13-Oligo for 24h.

Table 5.1. shows the all peaks which changed for this study and their interpretations.

Table 5.1. The spectral interpretations.

Peak	Interpretation
545 cm^{-1}	S-S
548 cm^{-1}	S-S
552 cm^{-1}	S-S
555 cm^{-1}	S-S
576 cm^{-1}	Phosphatidylinositol
585 cm^{-1}	PO$_4$
589 cm^{-1}	Symmetric stretching vibration of $v4$PO$_4^{-3}$
620 cm^{-1}	C-C twist aromatic ring
640 cm^{-1}	C-S stretching & C-C twisting of proteins
646 cm^{-1}	C-C twisting mode of tyrosine
656 cm^{-1}	Guanine
662 cm^{-1}	C-S stretching mode of cystine
678 cm^{-1}	Ring breathing modes in the DNA bases
682 cm^{-1}	C-S
687 cm^{-1}	C-N
689 cm^{-1}	C-N
717 cm^{-1}	C-N (membrane phospholipids head)
725 cm^{-1}	A (ring breathing mode of DNA/RNA bases)
728 cm^{-1}	C-C stretching, proline
729 cm^{-1}	Adenine
733 cm^{-1}	Phosphatidylserine
755 cm^{-1}	Symmetric breathing of tryptophan
760 cm^{-1}	Ring breathing tryptophan (proteins)
800 cm^{-1}	Phosphate ion interactions
813 cm^{-1}	Phosphate: v(OPO)
884 cm^{-1}	Proteins, including collagen I
890 cm^{-1}	Protein bands
960 cm^{-1}	Symmetric stretching vibration of PO$_4$
1031 cm^{-1}	Phenylalanine, C-N stretching of proteins
1064 cm^{-1}	Skeletal C-C stretch of lipids
1172 cm^{-1}	Tyrosine (protein assignment)
1203 cm^{-1}	Amide III
1223 cm^{-1}	Cellular nucleic acids
1224 cm^{-1}	Amide III
1228 cm^{-1}	Amide III
1230 cm^{-1}	Amide III
1247 cm^{-1}	Amide III
1260 cm^{-1}	Amide III
1265 cm^{-1}	Amide III
1266 cm^{-1}	Amide III
1269 cm^{-1}	Amide III

1275 cm^{-1}	Amide III
1278 cm^{-1}	Amide III
1280 cm^{-1}	Amide III
1296 cm^{-1}	Amide III
1302 cm^{-1}	Amide III
1317 cm^{-1}	Amide III
1319 cm^{-1}	Amide III
1320 cm^{-1}	Amide III
1337 cm^{-1}	Amide III
1356 cm^{-1}	Guanine
1420 cm^{-1}	Nucleic Acids
1445 cm^{-1}	CH$_2$ deformation

6. CONCLUSION AND FUTURE PERSPECTIVE

SERS has emerged as a technique to analyze single-cells without labeling. In this study, it was shown that using different size, surface chemistry, and incubation time for AuNPs had an influence on the obtained SERS spectra from single cells. As part of an ongoing effort in our research group where, the spectral changes on cellular SERS spectra are investigated, it was aimed to investigate SERS as a possible nano-sensing tool for tracing biochemical changes in a single cell. Thus, effects of AuNPs50, AuNPs50-Oligo, mixture of AuNPs50 and AuNPs13, and mixture of AuNPs50 and AuNPs13-Oligo on SERS activity upon their introduction to the cells were observed and it was found that size, surface chemistry and aggregation status of AuNPs play an important role.

When interpreting the observed spectral changes, one should carefully consider the cellular uptake processes of AuNPs. The source of spectral changes can be due to the differences in cellular uptake route, surface chemistry and aggregation status. The expectation was that both sizes of AuNPs and altered surface chemistry would cause difference in uptake route and biochemical processes taking place in the vicinity of the AuNPs. As indicated, AuNPs13 and AuNPs13-Oligo did not show any SERS activity. Therefore, AuNPs50 functioned as SERS active substrate. A 20-base long polyadenine oligonucleotide was used to coat the surface of both AuNPs sizes to change the surface chemistry. The difference in uptake profiles upon introduction of mixture of AuNPs (AuNPs50+AuNPs13 and AuNPs50+AuNPs13-Oligo) could result in differences in their aggregation status as well, which may also cause spectral variations.

After the endosomal uptake of the NPs, the endosomes are fused with the lysosome to form a hybrid structure, where some of the uptaken materials are digested. The hypothesis was that during this process changes in the vicinity of AuNPs could be monitored. If there is any possibility, the degradation of molecular structures bound to the AuNPs surfaces should be observed. In this study, as mentioned above, a 20-base long polyadenine was used to coat the AuNPs with the hope that upon degradation of polyadenine some changes at 729 cm^{-1} peak, which is attributed to adenine, could be observed.

The CV values of SERS spectra were used to evaluate the uptake progress and aggregation status of the AuNPs. Since the uptake of AuNPs is dynamic process, their aggregation status

continuously change until they settle down in the hybrid structure which could be one of the factors influencing the spectral variation. During the uptake process, proteins and receptors take very important roles for endosomal activity such as vesicle formation, motion, and endosome–lysosome fusion. Therefore, increase in the peak intensities corresponding to proteins was observed for all AuNPs treatments during the exposure time. For example, the increased peak intensities between 1200 cm^{-1} and 1400 cm^{-1} corresponding to Amide III bonds of proteins indicate the changes in secondary structure during exposure time. In addition, while the peak intensity at 646 cm^{-1} corresponding to C-C twisting mode of tyrosine increased, the peak intensity at 717 cm^{-1} attributed to C-N in membrane phospholipids decreased for all AuNPs treatments from 4 h to 24 h. In the first hours, AuNPs interact with membrane receptors during membrane wrapping and budding from the cell membrane. As the time pass, the vesicles transfer from the cell membrane into the cytosol. Meanwhile, early endosomes fuse with lysosomes, where the proteases are transferred into the endosome. Therefore, the increase in the peak intensities corresponding to protein structures and decrease in the peak intensities of phospholipid structures could indicate the motion of endosomes from early endosome to lysosomes.

The SERS spectra of obtained from each AuNPs treatments were compared to the same exposure time to investigate the effects of size and surface chemistry to relate the uptake process. The evaluation of the SERS spectra with the introduction of AuNPs50 and AuNPs50 + AuNPs13 reveal the interaction of lipids with SERS active surfaces while the introduction of AuNPs50-Oligo and AuNPs50 + AuNPs13-Oligo reveal the interaction of proteins with the SERS active surfaces at the initial incubation times. For example, peak intensities at 640 cm^{-1}, 662 cm^{-1} , and 755 cm^{-1} attributed to proteins increased for AuNPs50-Oligo treatment after 4 h treatment. These spectal changes were also observed for the treatment of AuNPs50 + AuNPs13-Oligo mixture. For 8 h treatment, an increase in the peak intensity at 1064 cm^{-1}, corresponding to C-C stretch of lipids, was observed for AuNPs50 while, a peak intensity increase at 890 cm^{-1} attributed to protein was observed for the AuNPs50-Oligo. The time dependent observed changes during 8 h in the SERS spectra of oligonucleotide modified AuNPs and unmodified AuNPs indicated that the surface chemistry strongly influenced the uptake of AuNPs and their aggregation status at the initial incubation times, possibly through the protein corona status of the AuNPs.

After 24 h, the spectral variation decreases as AuNPs settled down in the fused endosome-lysosome hybrid structures. The peaks at 552 cm^{-1} and 725 cm^{-1} attributed to adenine and phosphate, respectively, showed differences for each case of AuNPs treatment. While the peak at 552 cm^{-1} was observed for AuNPs50, AuNPs50-Oligo and AuNPs50 + AuNPs13-Oligo treatments, a shift from 552 cm^{-1} to 555 cm^{-1} was observed for the AuNPs50 + AuNPs13 treatment. In addition, the peak at 725 cm^{-1} was only observed for AuNPs50 + AuNPs13 treatment. The results were observed possibly due to acidification during endocytosis. In addition, aggregation status of AuNPs in endosomal-lysosomal compartments could be another reason for the enhancement of phosphate peak after 24 h.

In conclusion, this study shows that the surface chemistry, size and aggregation status of the SERS active AuNPs play important role for deciding their endosomal route and spectral patterns. Although the observed spectral changes are attempted to explain with the limited experimental study, the results indicate that further studies are necessary for full elucidation of the source of the observed spectral changes during the uptake of the AuNPs. In order to clarify status of the AuNPs as they enter into cells, a detailed TEM imaging study should be undertaken. In addition, performing the similar experiments with different cells lines will add invaluable insight to decipher the nature of the process taking place on the AuNPs surfaces as they travel into the cells.

REFERENCES

1.   Lodish H, Berk A, Kaiser C, Krieger M, Bretscher A, Ploegh H, et al. Transmembrane transport of ions and small molecules. Molecular cell biology, 7th edn Freeman, WH & Company, New York. 2012:473-516.

2.   Kanter I, Kalisky T. Single cell transcriptomics: methods and applications. Frontiers in oncology. 2015;5.

3.   Zhang X, Marjani SL, Hu Z, Weissman SM, Pan X, Wu S. Single-cell sequencing for precise cancer research: progress and prospects. Cancer research. 2016;76(6):1305-12.

4.   Li C, Klco JM, Helton NM, George DR, Mudd JL, Miller CA, et al. Genetic heterogeneity of induced pluripotent stem cells: results from 24 clones derived from a single C57BL/6 mouse. PloS one. 2015;10(3):e0120585.

5.   Stubbington MJ, Lönnberg T, Proserpio V, Clare S, Speak AO, Dougan G, et al. T cell fate and clonality inference from single cell transcriptomes. Nature methods. 2016;13(4):329.

6.   Heath JR, Ribas A, Mischel PS. Single cell analytic tools for drug discovery and development. Nature reviews Drug discovery. 2016;15(3):204.

7.   Shapiro E, Biezuner T, Linnarsson S. Single-cell sequencing-based technologies will revolutionize whole-organism science. Nature reviews Genetics. 2013;14(9):618.

8.   Yates JR, Ruse CI, Nakorchevsky A. Proteomics by mass spectrometry: approaches, advances, and applications. Annual review of biomedical engineering. 2009;11:49-79.

9.   Bendall SC, Simonds EF, Qiu P, El-ad DA, Krutzik PO, Finck R, et al. Single-cell mass cytometry of differential immune and drug responses across a human hematopoietic continuum. Science. 2011;332(6030):687-96.

10. Palonpon AF, Sodeoka M, Fujita K. Molecular imaging of live cells by Raman microscopy. Current opinion in chemical biology. 2013;17(4):708-15.

11. Puppels G, De Mul F, Otto C, Greve J, Robert-Nicoud M. Studying single living cells and chromosomes by confocal Raman microspectroscopy. Nature. 1990;347(6290):301.

12. Stiles PL, Dieringer JA, Shah NC, Van Duyne RP. Surface-enhanced Raman spectroscopy. Annu Rev Anal Chem. 2008;1:601-26.

13. Nabiev I, Morjani H, Manfait M. Selective analysis of antitumor drug interaction with living cancer cells as probed by surface-enhanced Raman spectroscopy. European biophysics journal. 1991;19(6):311-6.

14. Rejman J, Oberle V, Zuhorn IS, Hoekstra D. Size-dependent internalization of particles via the pathways of clathrin-and caveolae-mediated endocytosis. Biochemical Journal. 2004;377(1):159-69.

15. Conner SD, Schmid SL. Regulated portals of entry into the cell. Nature. 2003;422(6927):37-44.

16. Sabuncu AC, Grubbs J, Qian S, Abdel-Fattah TM, Stacey MW, Beskok A. Probing nanoparticle interactions in cell culture media. Colloids and Surfaces B: Biointerfaces. 2012;95:96-102.

17. Qiu Y, Liu Y, Wang L, Xu L, Bai R, Ji Y, et al. Surface chemistry and aspect ratio mediated cellular uptake of Au nanorods. Biomaterials. 2010;31(30):7606-19.

18. Chithrani BD, Ghazani AA, Chan WC. Determining the size and shape dependence of gold nanoparticle uptake into mammalian cells. Nano letters. 2006;6(4):662-8.

19. Ma N, Ma C, Li C, Wang T, Tang Y, Wang H, et al. Influence of nanoparticle shape, size, and surface functionalization on cellular uptake. Journal of nanoscience and nanotechnology. 2013;13(10):6485-98.

20.   Yue Z-G, Wei W, Lv P-P, Yue H, Wang L-Y, Su Z-G, et al. Surface charge affects cellular uptake and intracellular trafficking of chitosan-based nanoparticles. Biomacromolecules. 2011;12(7):2440-6.

21.   Enustun B, Turkevich J. Coagulation of colloidal gold. Journal of the American chemical society. 1963;85(21):3317-28.

22.   Kleinman SL, Frontiera RR, Henry A-I, Dieringer JA, Van Duyne RP. Creating, characterizing, and controlling chemistry with SERS hot spots. Physical Chemistry Chemical Physics. 2013;15(1):21-36.

23.   Zhang L, Cui X, Schmitt K, Hubert R, Navidi W, Arnheim N. Whole genome amplification from a single cell: implications for genetic analysis. Proceedings of the National Academy of Sciences. 1992;89(13):5847-51.

24.   Acinas SG, Sarma-Rupavtarm R, Klepac-Ceraj V, Polz MF. PCR-induced sequence artifacts and bias: insights from comparison of two 16S rRNA clone libraries constructed from the same sample. Applied and environmental microbiology. 2005;71(12):8966-9.

25.   Zong C, Lu S, Chapman AR, Xie XS. Genome-wide detection of single-nucleotide and copy-number variations of a single human cell. Science. 2012;338(6114):1622-6.

26.   Gawad C, Koh W, Quake SR. Single-cell genome sequencing: current state of the science. Nature reviews Genetics. 2016;17(3):175.

27.   Lao KQ, Tang F, Barbacioru C, Wang Y, Nordman E, Lee C, et al. mRNA-Sequencing Whole Transcriptome Analysis of a Single Cell on the SOLiD™ System. Journal of biomolecular techniques: JBT. 2009;20(5):266.

28.   Treutlein B, Brownfield DG, Wu AR, Neff NF, Mantalas GL, Espinoza FH, et al. Reconstructing lineage hierarchies of the distal lung epithelium using single cell RNA-seq. Nature. 2014;509(7500):371.

29.   Patel AP, Tirosh I, Trombetta JJ, Shalek AK, Gillespie SM, Wakimoto H, et al. Single-cell RNA-seq highlights intratumoral heterogeneity in primary glioblastoma. Science. 2014;344(6190):1396-401.

30.   Shalek AK, Satija R, Adiconis X, Gertner RS, Gaublomme JT, Raychowdhury R, et al. Single-cell transcriptomics reveals bimodality in expression and splicing in immune cells. Nature. 2013;498(7453):236.

31.   Wu AR, Neff NF, Kalisky T, Dalerba P, Treutlein B, Rothenberg ME, et al. Quantitative assessment of single-cell RNA-sequencing methods. Nature methods. 2014;11(1):41.

32.   Nawy T. Single-cell sequencing: a brief overview of how to derive a genome or transcriptome from a single cell. Nature methods. 2014;11(1):18-9.

33.   Olive PL, Banáth JP, Durand RE. Heterogeneity in radiation-induced DNA damage and repair in tumor and normal cells measured using the" comet" assay. Radiation research. 1990;122(1):86-94.

34.   Ostling O, Johanson K. Microelectrophoretic study of radiation-induced DNA damages in individual mammalian cells. Biochemical and biophysical research communications. 1984;123(1):291-8.

35.   Whittal RM, Keller BO, Li L. Nanoliter chemistry combined with mass spectrometry for peptide mapping of proteins from single mammalian cell lysates. Analytical chemistry. 1998;70(24):5344-7.

36.   Shrestha B, Vertes A. In situ metabolic profiling of single cells by laser ablation electrospray ionization mass spectrometry. Analytical Chemistry. 2009;81(20):8265-71.

37.   Love JC, Ronan JL, Grotenbreg GM, van der Veen AG, Ploegh HL. A microengraving method for rapid selection of single cells producing antigen-specific antibodies. Nature biotechnology. 2006;24(6):703-7.

38.   Torres AJ, Contento RL, Gordo S, Wucherpfennig KW, Love JC. Functional single-cell analysis of T-cell activation by supported lipid bilayer-tethered ligands on arrays of nanowells. Lab on a Chip. 2013;13(1):90-9.

39.   Hughes AJ, Spelke DP, Xu Z, Kang C-C, Schaffer DV, Herr AE. Single-cell western blotting. Nature methods. 2014;11(7):749-55.

40.   Angelo M, Bendall SC, Finck R, Hale MB, Hitzman C, Borowsky AD, et al. Multiplexed ion beam imaging of human breast tumors. Nature medicine. 2014;20(4):436-42.

41.   Kim KS, Cho CH, Park EK, Jung M-H, Yoon K-S, Park H-K. AFM-detected apoptotic changes in morphology and biophysical property caused by paclitaxel in Ishikawa and HeLa cells. PloS one. 2012;7(1):e30066.

42.   Henriques R, Griffiths C, Hesper Rego E, Mhlanga MM. PALM and STORM: Unlocking live-cell super-resolution. Biopolymers. 2011;95(5):322-31.

43.   Raman C, Krishnan K. A new type of secondary radiation [Reproduced from Nature, 1928, 121, 501–502]. Current Science. 1998;74(4):381-.

44.   Wokaun A. B. Schrader: Infrared and Raman Spectroscopy-Methods and Applications. VCH, Weinheim, 1995, DM 298,-, ISBN 3-527-26446-9. Berichte der Bunsengesellschaft für physikalische Chemie. 1996;100(7):1268-.

45.   Wertz J. Electron spin resonance: elementary theory and practical applications: Springer Science & Business Media; 2012.

46.   Placzek G. Rayleigh-streuung und Raman-effekt: Akad. Verlag-Ges.; 1934.

47.   Howat WJ, Wilson BA. Tissue fixation and the effect of molecular fixatives on downstream staining procedures. Methods. 2014;70(1):12-9.

48.   Uzunbajakava N, Lenferink A, Kraan Y, Volokhina E, Vrensen G, Greve J, et al. Nonresonant confocal Raman imaging of DNA and protein distribution in apoptotic cells. Biophysical journal. 2003;84(6):3968-81.

49.   Uzunbajakava N, Lenferink A, Kraan Y, Willekens B, Vrensen G, Greve J, et al. Nonresonant Raman imaging of protein distribution in single human cells. Biopolymers. 2003;72(1):1-9.

50.   van Manen H-J, Kraan YM, Roos D, Otto C. Single-cell Raman and fluorescence microscopy reveal the association of lipid bodies with phagosomes in leukocytes. Proceedings of the National Academy of Sciences of the United States of America. 2005;102(29):10159-64.

51.   Okada M, Smith NI, Palonpon AF, Endo H, Kawata S, Sodeoka M, et al. Label-free Raman observation of cytochrome c dynamics during apoptosis. Proceedings of the National Academy of Sciences. 2012;109(1):28-32.

52.   Matthäus C, Boydston-White S, Miljković M, Romeo M, Diem M. Raman and infrared microspectral imaging of mitotic cells. Applied spectroscopy. 2006;60(1):1-8.

53.   Haka AS, Shafer-Peltier KE, Fitzmaurice M, Crowe J, Dasari RR, Feld MS. Identifying microcalcifications in benign and malignant breast lesions by probing differences in their chemical composition using Raman spectroscopy. Cancer research. 2002;62(18):5375-80.

54.   Chan JW, Taylor DS, Thompson DL. The effect of cell fixation on the discrimination of normal and leukemia cells with laser tweezers Raman spectroscopy. Biopolymers. 2009;91(2):132-9.

55.   Draux F, Gobinet C, Sulé-Suso J, Trussardi A, Manfait M, Jeannesson P, et al. Raman spectral imaging of single cancer cells: probing the impact of sample fixation methods. Analytical and bioanalytical chemistry. 2010;397(7):2727-37.

56.   Meade AD, Clarke C, Draux F, Sockalingum GD, Manfait M, Lyng FM, et al. Studies of chemical fixation effects in human cell lines using Raman microspectroscopy. Analytical and bioanalytical chemistry. 2010;396(5):1781-91.

57.   Schie IW, Alber L, Gryshuk AL, Chan JW. Investigating drug induced changes in single, living lymphocytes based on Raman micro-spectroscopy. Analyst. 2014;139(11):2726-33.

58.   Konorov SO, Schulze HG, Piret JM, Blades MW, Turner RF. Label-free determination of the cell cycle phase in human embryonic stem cells by Raman microspectroscopy. Analytical chemistry. 2013;85(19):8996-9002.

59.   Smith E, Dent G. Modern Raman spectroscopy: a practical approach: John Wiley & Sons; 2013.

60.   Smith ZJ, Huser TR, Wachsmann-Hogiu S. Raman scattering in pathology. Analytical Cellular Pathology. 2012;35(3):145-63.

61.   Lee P, Meisel D. Adsorption and surface-enhanced Raman of dyes on silver and gold sols. The Journal of Physical Chemistry. 1982;86(17):3391-5.

62.   Campion A, Kambhampati P. Surface-enhanced Raman scattering. Chemical Society Reviews. 1998;27(4):241-50.

63.   Fleischmann M, Hendra PJ, McQuillan AJ. Raman spectra of pyridine adsorbed at a silver electrode. Chemical Physics Letters. 1974;26(2):163-6.

64.   Jeanmaire DL, Van Duyne RP. Surface Raman spectroelectrochemistry: Part I. Heterocyclic, aromatic, and aliphatic amines adsorbed on the anodized silver electrode. Journal of Electroanalytical Chemistry and Interfacial Electrochemistry. 1977;84(1):1-20.

65.   Schatz GC. Theoretical studies of surface enhanced Raman scattering. Accounts of Chemical Research. 1984;17(10):370-6.

66.   Morton SM, Jensen L. Understanding the molecule− surface chemical coupling in SERS. Journal of the American Chemical Society. 2009;131(11):4090-8.

67.   Camden JP, Dieringer JA, Wang Y, Masiello DJ, Marks LD, Schatz GC, et al. Probing the structure of single-molecule surface-enhanced Raman scattering hot spots. Journal of the American Chemical Society. 2008;130(38):12616-7.

68.   Yamada H, Yamamoto Y, Tani N. Surface-enhanced raman scattering (SERS) of adsorbed molecules on smooth surfaces of metals and a metal oxide. Chemical Physics Letters. 1982;86(4):397-400.

69.   Yamada H, Yamamoto Y. Surface enhanced Raman scattering (SERS) of chemisorbed species on various kinds of metals and semiconductors. Surface science. 1983;134(1):71-90.

70.   Ueba H. Theory of Raman scattering from molecules adsorbed at semiconductor surfaces. Surface science. 1983;131(2-3):328-46.

71.   Mou C, He T, Wang X, Liu F-Z, Jiang J-S, Chen L-W. Surface Enhanced Raman Scattering (SERs) from H~ 2TSPP and Ag (II) TSPP Adsorbed on Uniform Fe~ 3O~ 4 Colloids. ACTA PHYSICOCHIMICA SINICA. 1996;12:841-4.

72.   Yanfei W, Hailong H, Shengyu J, Yunxin W, Zhihua S, Bing Z, et al. Enhanced Raman scattering as a probe for 4-mercaptopyridine surface-modified copper oxide nanocrystals. Analytical sciences. 2007;23(7):787-91.

73.   Wang Y, Zhang J, Jia H, Li M, Zeng J, Yang B, et al. Mercaptopyridine surface-functionalized CdTe quantum dots with enhanced Raman scattering properties. The Journal of Physical Chemistry C. 2008;112(4):996-1000.

74.   Fu X, Pan Y, Wang X, Lombardi JR. Quantum confinement effects on charge-transfer between PbS quantum dots and 4-mercaptopyridine. The Journal of chemical physics. 2011;134(2):024707.

75.   Xie L, Ling X, Fang Y, Zhang J, Liu Z. Graphene as a substrate to suppress fluorescence in resonance Raman spectroscopy. Journal of the American Chemical Society. 2009;131(29):9890-1.

76.   Ghosh SK, Pal T. Interparticle coupling effect on the surface plasmon resonance of gold nanoparticles: from theory to applications. Chemical reviews. 2007;107(11):4797-862.

77.   Kong X, Yu Q, Zhang X, Du X, Gong H, Jiang H. Synthesis and application of surface enhanced Raman scattering (SERS) tags of Ag@ SiO 2 core/shell nanoparticles in protein detection. Journal of Materials Chemistry. 2012;22(16):7767-74.

78.   Mulvaney SP, Musick MD, Keating CD, Natan MJ. Glass-coated, analyte-tagged nanoparticles: a new tagging system based on detection with surface-enhanced Raman scattering. Langmuir. 2003;19(11):4784-90.

79.   Kong X, Yu Q, Lv Z, Du X. Tandem Assays of Protein and Glucose with Functionalized Core/Shell Particles Based on Magnetic Separation and Surface-Enhanced Raman Scattering. Small. 2013;9(19):3259-64.

80.   Nie S, Emory SR. Probing single molecules and single nanoparticles by surface-enhanced Raman scattering. science. 1997;275(5303):1102-6.

81.   Ni J, Lipert RJ, Dawson GB, Porter MD. Immunoassay readout method using extrinsic Raman labels adsorbed on immunogold colloids. Analytical Chemistry. 1999;71(21):4903-8.

82.   Jackson JB, Halas NJ. Surface-enhanced Raman scattering on tunable plasmonic nanoparticle substrates. Proceedings of the National Academy of Sciences. 2004;101(52):17930-5.

83.   Alkilany AM, Murphy CJ. Toxicity and cellular uptake of gold nanoparticles: what we have learned so far? Journal of nanoparticle research. 2010;12(7):2313-33.

84.   Finkelstein A, Walz D, Batista V, Mizraji M, Roisman F, Misher A. Auranofin. New oral gold compound for treatment of rheumatoid arthritis. Annals of the rheumatic diseases. 1976;35(3):251-7.

85.   Connor EE, Mwamuka J, Gole A, Murphy CJ, Wyatt MD. Gold nanoparticles are taken up by human cells but do not cause acute cytotoxicity. Small. 2005;1(3):325-7.

86.   Goodman CM, McCusker CD, Yilmaz T, Rotello VM. Toxicity of gold nanoparticles functionalized with cationic and anionic side chains. Bioconjugate chemistry. 2004;15(4):897-900.

87.   Pan Y, Leifert A, Ruau D, Neuss S, Bornemann J, Schmid G, et al. Gold nanoparticles of diameter 1.4 nm trigger necrosis by oxidative stress and mitochondrial damage. Small. 2009;5(18):2067-76.

88.   Nikoobakht B, El-Sayed MA. Preparation and growth mechanism of gold nanorods (NRs) using seed-mediated growth method. Chemistry of Materials. 2003;15(10):1957-62.

89.   Creighton JA, Blatchford CG, Albrecht MG. Plasma resonance enhancement of Raman scattering by pyridine adsorbed on silver or gold sol particles of size comparable to the excitation wavelength. Journal of the Chemical Society, Faraday Transactions 2: Molecular and Chemical Physics. 1979;75:790-8.

90.   Jiang W, Kim BY, Rutka JT, Chan WC. Nanoparticle-mediated cellular response is size-dependent. Nature nanotechnology. 2008;3(3):145-50.

91.   Hall A, Nobes CD. Rho GTPases: molecular switches that control the organization and dynamics of the actin cytoskeleton. Philosophical Transactions of the Royal Society of London B: Biological Sciences. 2000;355(1399):965-70.

92.   Anderson RG. The caveolae membrane system. Annual review of biochemistry. 1998;67(1):199-225.

93.   Hirst J, Robinson MS. Clathrin and adaptors. Biochimica et Biophysica Acta (BBA)-Molecular Cell Research. 1998;1404(1):173-93.

94.   Anderson RG, Jacobson K. A role for lipid shells in targeting proteins to caveolae, rafts, and other lipid domains. Science. 2002;296(5574):1821-5.

95.   Jiang Y, Huo S, Mizuhara T, Das R, Lee Y-W, Hou S, et al. The interplay of size and surface functionality on the cellular uptake of sub-10 nm gold nanoparticles. ACS nano. 2015;9(10):9986-93.

96.   Cho EC, Xie J, Wurm PA, Xia Y. Understanding the role of surface charges in cellular adsorption versus internalization by selectively removing gold nanoparticles on the cell surface with a I2/KI etchant. Nano letters. 2009;9(3):1080-4.

97.   Bao H, Zhang Q, Xu H, Yan Z. Effects of nanoparticle size on antitumor activity of 10-hydroxycamptothecin-conjugated gold nanoparticles: in vitro and in vivo studies. International journal of nanomedicine. 2016;11:929.

98.   Cho EC, Liu Y, Xia Y. A simple spectroscopic method for differentiating cellular uptakes of gold nanospheres and nanorods from their mixtures. Angewandte Chemie International Edition. 2010;49(11):1976-80.

99.   Au L, Zhang Q, Cobley CM, Gidding M, Schwartz AG, Chen J, et al. Quantifying the cellular uptake of antibody-conjugated Au nanocages by two-photon microscopy and inductively coupled plasma mass spectrometry. ACS nano. 2009;4(1):35-42.

100.   Hauck TS, Ghazani AA, Chan WC. Assessing the effect of surface chemistry on gold nanorod uptake, toxicity, and gene expression in mammalian cells. Small. 2008;4(1):153-9.

101.   Bantz KC, Meyer AF, Wittenberg NJ, Im H, Kurtuluş Ö, Lee SH, et al. Recent progress in SERS biosensing. Physical Chemistry Chemical Physics. 2011;13(24):11551-67.

102.   Clemens G, Hands JR, Dorling KM, Baker MJ. Vibrational spectroscopic methods for cytology and cellular research. Analyst. 2014;139(18):4411-44.

103.   Ellis DI, Cowcher DP, Ashton L, O'Hagan S, Goodacre R. Illuminating disease and enlightening biomedicine: Raman spectroscopy as a diagnostic tool. Analyst. 2013;138(14):3871-84.

104.   Shanmukh S, Jones L, Driskell J, Zhao Y, Dluhy R, Tripp RA. Rapid and sensitive detection of respiratory virus molecular signatures using a silver nanorod array SERS substrate. Nano letters. 2006;6(11):2630-6.

105.   Premasiri W, Moir D, Klempner M, Krieger N, Jones G, Ziegler L. Characterization of the surface enhanced Raman scattering (SERS) of bacteria. The journal of physical chemistry B. 2005;109(1):312-20.

106.   Fan Z, Kanchanapally R, Ray PC. Hybrid graphene oxide based ultrasensitive SERS probe for label-free biosensing. The Journal of Physical Chemistry Letters. 2013;4(21):3813-8.

107.   Barhoumi A, Halas NJ. Label-free detection of DNA hybridization using surface enhanced Raman spectroscopy. Journal of the American Chemical Society. 2010;132(37):12792-3.

108.   Sinha L, Wang Y, Yang C, Khan A, Brankov JG, Liu JT, et al. Quantification of the binding potential of cell-surface receptors in fresh excised specimens via dual-probe modeling of SERS nanoparticles. Scientific reports. 2015;5:8582.

109.   Li Y, Qi X, Lei C, Yue Q, Zhang S. Simultaneous SERS detection and imaging of two biomarkers on the cancer cell surface by self-assembly of branched DNA–gold nanoaggregates. Chemical Communications. 2014;50(69):9907-9.

110.   Hu Q, Tay L-L, Noestheden M, Pezacki JP. Mammalian cell surface imaging with nitrile-functionalized nanoprobes: biophysical characterization of aggregation and

polarization anisotropy in SERS imaging. Journal of the American Chemical Society. 2007;129(1):14-5.

111.   Kneipp K, Haka AS, Kneipp H, Badizadegan K, Yoshizawa N, Boone C, et al. Surface-enhanced Raman spectroscopy in single living cells using gold nanoparticles. Applied Spectroscopy. 2002;56(2):150-4.

112.   Huang X, El-Sayed IH, Qian W, El-Sayed MA. Cancer cells assemble and align gold nanorods conjugated to antibodies to produce highly enhanced, sharp, and polarized surface Raman spectra: a potential cancer diagnostic marker. Nano letters. 2007;7(6):1591-7.

113.   Kuku G, Saricam M, Akhatova F, Danilushkina A, Fakhrullin R, Culha M. Surface-enhanced raman scattering to evaluate nanomaterial cytotoxicity on living cells. Analytical Chemistry. 2016;88(19):9813-20.

114.   Xu L, Kuang H, Xu C, Ma W, Wang L, Kotov NA. Regiospecific plasmonic assemblies for in situ Raman spectroscopy in live cells. Journal of the American Chemical Society. 2012;134(3):1699-709.

115.   Jaworska A, Jamieson LE, Malek K, Campbell CJ, Choo J, Chlopicki S, et al. SERS-based monitoring of the intracellular pH in endothelial cells: the influence of the extracellular environment and tumour necrosis factor-α. Analyst. 2015;140(7):2321-9.

116.   Zheng X-S, Hu P, Cui Y, Zong C, Feng J-M, Wang X, et al. BSA-coated nanoparticles for improved SERS-based intracellular pH sensing. Analytical chemistry. 2014;86(24):12250-7.

117.   Pissuwan D, Hattori Y. Detection of Adhesion Molecules on Inflamed Macrophages at Early-Stage Using SERS Probe Gold Nanorods. Nano-Micro Letters. 2017;9(1):8.

118.   Shi M, Zheng J, Liu C, Tan G, Qing Z, Yang S, et al. SERS assay of telomerase activity at single-cell level and colon cancer tissues via quadratic signal amplification. Biosensors and Bioelectronics. 2016;77:673-80.

119. Zhang Q, Lu X, Tang P, Zhang D, Tian J, Zhong L. Gold Nanoparticle (AuNP)-Based Surface-Enhanced Raman Scattering (SERS) Probe of Leukemic Lymphocytes. Plasmonics. 2016;11(5):1361-8.

120. Fasolato C, Giantulli S, Silvestri I, Mazzarda F, Toumia Y, Ripanti F, et al. Folate-based single cell screening using surface enhanced Raman microimaging. Nanoscale. 2016;8(39):17304-13.

121. Hossain M, Cho H-Y, Choi J-W. Gold Nanosphere-Deposited Substrate for Distinguishing of Breast Cancer Subtypes Using Surface-Enhanced Raman Spectroscopy. Journal of Nanoscience and Nanotechnology. 2016;16(6):6299-303.

122. Jimenez de Aberasturi D, Serrano-Montes AB, Langer J, Henriksen-Lacey M, Parak WJ, Liz-Marzán LM. Surface enhanced raman scattering encoded gold nanostars for multiplexed cell discrimination. Chemistry of Materials. 2016;28(18):6779-90.

123. Kim T-H, Lee K-B, Choi J-W. 3D graphene oxide-encapsulated gold nanoparticles to detect neural stem cell differentiation. Biomaterials. 2013;34(34):8660-70.

124. El-Said WA, Kim SU, Choi J-W. Monitoring in vitro neural stem cell differentiation based on surface-enhanced Raman spectroscopy using a gold nanostar array. Journal of Materials Chemistry C. 2015;3(16):3848-59.

125. Yousif LF, Stewart KM, Kelley SO. Targeting Mitochondria with Organelle-Specific Compounds: Strategies and Applications. ChemBioChem. 2009;10(12):1939-50.

126. Oyelere AK, Chen PC, Huang X, El-Sayed IH, El-Sayed MA. Peptide-conjugated gold nanorods for nuclear targeting. Bioconjugate chemistry. 2007;18(5):1490-7.

127. Huefner A, Kuan W-L, Barker RA, Mahajan S. Intracellular SERS nanoprobes for distinction of different neuronal cell types. Nano letters. 2013;13(6):2463-70.

128.   Austin LA, Kang B, El-Sayed MA. A new nanotechnology technique for determining drug efficacy using targeted plasmonically enhanced single cell imaging spectroscopy. Journal of the American Chemical Society. 2013;135(12):4688-91.

129.   Aioub M, Kang B, Mackey MA, El-Sayed MA. Biological targeting of plasmonic nanoparticles improves cellular imaging via the enhanced scattering in the aggregates formed. The journal of physical chemistry letters. 2014;5(15):2555-61.

130.   Mirkin CA, Letsinger RL, Mucic RC, Storhoff JJ. A DNA-based method for rationally assembling nanoparticles into macroscopic materials. Nature. 1996;382(6592):607.

131.   Murdock RC, Braydich-Stolle L, Schrand AM, Schlager JJ, Hussain SM. Characterization of nanomaterial dispersion in solution prior to in vitro exposure using dynamic light scattering technique. Toxicological sciences. 2008;101(2):239-53.

132.   Abdelhalim MAK, Mady MM, Ghannam MM. Physical properties of different gold nanoparticles: ultraviolet-visible and fluorescence measurements. J Nanomed Nanotechol. 2012;3(3):178-94.

133.   Albanese A, Chan WC. Effect of gold nanoparticle aggregation on cell uptake and toxicity. ACS nano. 2011;5(7):5478-89.

134.   Kneipp J, Kneipp H, McLaughlin M, Brown D, Kneipp K. In vivo molecular probing of cellular compartments with gold nanoparticles and nanoaggregates. Nano Letters. 2006;6(10):2225-31.

135.   Naumann D, editor Infrared and NIR Raman spectroscopy in medical microbiology. BiOS'98 International Biomedical Optics Symposium; 1998: International Society for Optics and Photonics.

136.   Stone N, Kendall C, Shepherd N, Crow P, Barr H. Near-infrared Raman spectroscopy for the classification of epithelial pre-cancers and cancers. Journal of Raman spectroscopy. 2002;33(7):564-73.

137.   Notingher I, Green C, Dyer C, Perkins E, Hopkins N, Lindsay C, et al. Discrimination between ricin and sulphur mustard toxicity in vitro using Raman spectroscopy. Journal of the Royal Society Interface. 2004;1(1):79-90.

138.   Ruiz-Chica A, Medina M, Sanchez-Jimenez F, Ramirez F. Characterization by Raman spectroscopy of conformational changes on guanine–cytosine and adenine–thymine oligonucleotides induced by aminooxy analogues of spermidine. Journal of Raman spectroscopy. 2004;35(2):93-100.

139.   Cheng WT, Liu MT, Liu HN, Lin SY. Micro-Raman spectroscopy used to identify and grade human skin pilomatrixoma. Microscopy research and technique. 2005;68(2):75-9.

140.   Faolain EO, Hunter MB, Byrne JM, Kelehan P, McNamara M, Byrne HJ, et al. A study examining the effects of tissue processing on human tissue sections using vibrational spectroscopy. Vibrational Spectroscopy. 2005;38(1):121-7.

141.   Chan JW, Taylor DS, Zwerdling T, Lane SM, Ihara K, Huser T. Micro-Raman spectroscopy detects individual neoplastic and normal hematopoietic cells. Biophysical journal. 2006;90(2):648-56.

142.   Büchner T, Drescher D, Traub H, Schrade P, Bachmann S, Jakubowski N, et al. Relating surface-enhanced Raman scattering signals of cells to gold nanoparticle aggregation as determined by LA-ICP-MS micromapping. Analytical and bioanalytical chemistry. 2014;406(27):7003-14.

143.   Giljohann DA, Seferos DS, Patel PC, Millstone JE, Rosi NL, Mirkin CA. Oligonucleotide loading determines cellular uptake of DNA-modified gold nanoparticles. Nano letters. 2007;7(12):3818-21.

144.   Binoy J, Abraham JP, Joe IH, Jayakumar V, Pettit G, Nielsen OF. NIR-FT Raman and FT-IR spectral studies and ab initio calculations of the anti-cancer drug combretastatin-A4. Journal of Raman Spectroscopy. 2004;35(11):939-46.

145.   Shetty G, Kendall C, Shepherd N, Stone N, Barr H. Raman spectroscopy: elucidation of biochemical changes in carcinogenesis of oesophagus. British journal of cancer. 2006;94(10):1460-4.

146.   Kang B, Austin LA, El-Sayed MA. Observing real-time molecular event dynamics of apoptosis in living cancer cells using nuclear-targeted plasmonically enhanced Raman nanoprobes. ACS nano. 2014;8(5):4883-92.

147.   Takei K, Haucke V. Clathrin-mediated endocytosis: membrane factors pull the trigger. Trends in cell biology. 2001;11(9):385-91.

148.   Kneipp J, Kneipp H, Wittig B, Kneipp K. Following the dynamics of pH in endosomes of live cells with SERS nanosensors. The Journal of Physical Chemistry C. 2010;114(16):7421-6.

149.   Huotari J, Helenius A. Endosome maturation. The EMBO journal. 2011;30(17):3481-500.